REPORT DOCUMENTATION PAGE

1

Form Approved OMB NO. 0704-0188

1. REPORT DATE (DD-MM-YYYY)	2. REPORT TYPE	3. DATES COVERED (From - To)
29-08-2014	MS Thesis	-

4. TITLE AND SUBTITLE
NONLOCAL OPTICAL RESPONSE OF PLASMONIC NANOWIRE METAMATERIALS

5a. CONTRACT NUMBER
W911NF-12-1-0533

5b. GRANT NUMBER

5c. PROGRAM ELEMENT NUMBER
611102

6. AUTHORS
Brian Wells

5d. PROJECT NUMBER

5e. TASK NUMBER

5f. WORK UNIT NUMBER

7. PERFORMING ORGANIZATION NAMES AND ADDRESSES
University of Massachusetts - Lowell
Office of Research Administration
600 Suffolk Street, Suite 226
Lowell, MA 01854 -3643

8. PERFORMING ORGANIZATION REPORT NUMBER

9. SPONSORING/MONITORING AGENCY NAME(S) AND ADDRESS (ES)
U.S. Army Research Office
P.O. Box 12211
Research Triangle Park, NC 27709-2211

10. SPONSOR/MONITOR'S ACRONYM(S)
ARO

11. SPONSOR/MONITOR'S REPORT NUMBER(S)
61388-PH.11

12. DISTRIBUTION AVAILIBILITY STATEMENT
Approved for public release; distribution is unlimited.

13. SUPPLEMENTARY NOTES
The views, opinions and/or findings contained in this report are those of the author(s) and should not contrued as an official Department of the Army position, policy or decision, unless so designated by other documentation.

14. ABSTRACT
Nanowire metamaterials are a class of composite photonic media formed by an array of aligned plasmonic nanowires embedded in a dielectric matrix. Depending on exact composition, geometry, and excitation wavelength, nanowire structures are known to exhibit elliptical, hyperbolic, or epsilon-near-zero (ENZ) responses. In the ENZ regime, optical response of the composite becomes strongly nonlocal. Excitation of an additional wave, caused by nonlocality, has been experimentally demonstrated in nanowire-based metamaterials. In this thesis, a computational study of the nonlocal optical response in plasmonic nanowire arrays has been conducted to better

15. SUBJECT TERMS
Plasmonics, metamaterials, optical nonlocality

16. SECURITY CLASSIFICATION OF:			17. LIMITATION OF ABSTRACT	15. NUMBER OF PAGES	19a. NAME OF RESPONSIBLE PERSON
a. REPORT	b. ABSTRACT	c. THIS PAGE			Viktor Podolskiy
UU	UU	UU	UU		19b. TELEPHONE NUMBER 978-934-3398

Report Title

NONLOCAL OPTICAL RESPONSE OF PLASMONIC NANOWIRE METAMATERIALS

ABSTRACT

Nanowire metamaterials are a class of composite photonic media formed by an array of aligned plasmonic nanowires embedded in a dielectric matrix. Depending on exact composition, geometry, and excitation wavelength, nanowire structures are known to exhibit elliptical, hyperbolic, or epsilon-near-zero (ENZ) responses. In the ENZ regime, optical response of the composite becomes strongly nonlocal. Excitation of an additional wave, caused by nonlocality, has been experimentally demonstrated in nanowire-based metamaterials. In this thesis, a computational study of the nonlocal optical response in plasmonic nanowire arrays has been conducted to better understand such materials. The results of this computational study were used to develop an analytical technique that provides an adequate description of the optical response of wire based metamaterials. This formalism combines the local and nonlocal effective-medium theories often used to describe the optics of nanowire composites. It provides insight into the origin of the additional wave and allows implementation of additional boundary conditions. This approach can be straightforwardly extended to describe the optics for numerious plasmonic structures

NONLOCAL OPTICAL RESPONSE OF PLASMONIC NANOWIRE METAMATERIALS

BY

BRIAN MICHAEL WELLS
B.A. (PHYSICS), CLARK UNIVERSITY, WORCESTER, MASSACHUSETTS

SUBMITTED IN PARTIAL FULFILLMENT OF THE REQUIREMENTS
FOR THE DEGREE OF MASTER OF SCIENCE
DEPARTMENT OF PHYSICS AND APPLIED PHYSICS
UNIVERSITY OF MASSACHUSETTS, LOWELL

_____

Signature of Author

Signature of Thesis Supervisor:

_____

Dr. Viktor A. Podolskiy

Signatures of Thesis Committee Members:

_____

Dr. James J. Egan

_____

Dr. Wei Guo

Abstract of Thesis:

Nanowire metamaterials are a class of composite photonic media formed by an array of aligned plasmonic nanowires embedded in a dielectric matrix. Depending on exact composition, geometry, and excitation wavelength, nanowire structures are known to exhibit elliptical, hyperbolic, or epsilon-near-zero (ENZ) responses. In the ENZ regime, optical response of the composite becomes strongly nonlocal. Excitation of an additional wave, caused by nonlocality, has been experimentally demonstrated in nanowire-based metamaterials. In this thesis, a computational study of the nonlocal optical response in plasmonic nanowire arrays has been conducted to better understand such materials. The results of this computational study were used to develop an analytical technique that provides an adequate description of the optical response of wire based metamaterials. This formalism combines the local and nonlocal effective-medium theories often used to describe the optics of nanowire composites. It provides insight into the origin of the additional wave and allows implementation of additional boundary conditions. This approach can be straightforwardly extended to describe the optics for numerious plasmonic structures.

Acknowledgements

I would like to express my most sincere gratitude to my advisor, Dr. Viktor Podolskiy, for his motivation, immense knowledge, compassion, patience, and for providing me with an exceptional atmosphere for doing this fascinating and exciting research. His guidance helped me during all of the research and writing process of this thesis. I am very appreciative of him as both an advisor and mentor for my graduate studies.

Besides my advisor, I would like to thank the rest of my thesis committee: Dr. James Egan and Dr. Wei Guo, for their encouragement, insightful comments, and hard questions. I would also like to thank our experimental collaborator Dr. Anatoly Zayats from Kings College, London, for his valuable insight regarding the experimental results and the countless times he would help review papers either for publications or conferences.

I thank my fellow labmates Sandeep Inampudi and Christopher Roberts for all their support and the many times when I needed to brainstorm new ideas or had any questions regarding this research. They were always there.

I would also like to thank the funding agencies for providing financial support. This research has been partially supported by the US Army Research Office (grant # W911NF-12-1-0533), EPSRC (UK), and the ERC iPLASMM project (321268).

I would like to thank my family, especially my parents Donna Pope and Kevin Wells, and my grandparents Leonard and Judy Hutchinson, who have always given me their unequivocal support. As always, my mere expression of thanks does not suffice.

Finally, I would like to thank Emily Van Ness, who has been there, keeping me focused and motivating me to do the very best in all that I do.

Contents

List of Figures

1 Introduction

Over the past several years, there has been an increased interest from the scientific community to further study and better understand metamaterials. Metamaterials are a class of composite materials artificially constructed to exhibit exceptional properties that are not readily found in nature. There are numerous applications in modern optics which can be realized through the study and understanding of light propagation within metamaterials. These range from imaging, sensing, and security, to solar power, optical information processing, and photonic circuits [1-9]

One such metamaterial that has recently attracted significant attention include nanowire-based composites, a class of materials formed by an array of aligned plasmonic nanowires embedded in a dielectric substrate (Fig 1.1). These wire materials are a sub-class of uniaxial metamaterials that have a homogeneous internal structure along one pre-selected direction. Due to relatively low loss and ease of fabrication, nanowire composites have found a multitude of applications in subwavelength imaging, biosensing, acousto-optics, and ultrafast all-optical processing, spanning visible to THz frequencies [10-15].

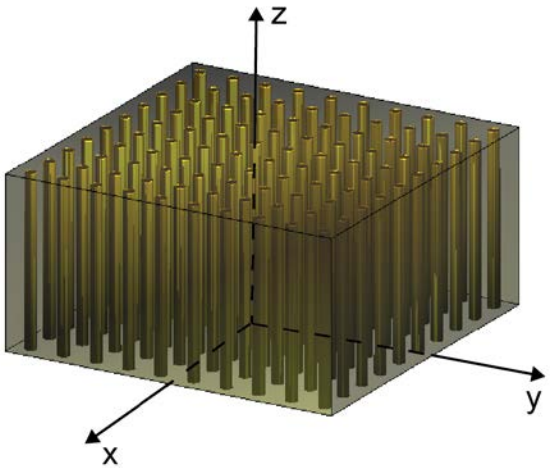

Figure 1.1: Schematic geometry of wire array.

Nanowire structures can be successfully fabricated using electrochemistry [7]. This process generally results in nanowire composites consisting of anodized alumina substrates with pre-etched holes filled with noble metals, such as gold (Au) [16]. For these types of materials, the radius *r* for the individual nanowires can be controlled between 10 and 100 *nm* with a separation distance *a* between 50 and ~300*nm*.

Not only do nanowire-based composites form the platform for practical applications, these materials have also gained attention due to their unusual and counter-intuitive optical properties. These behaviors include negative refraction, subwavelength confinement of optical radiation, and modulation of photonic density of states [17-21]. The unusual optical phenomena inside these nanowire-based structures can often be accredited to extremely large or vanishingly small values of the effective refractive index. It can be shown that at these extreme values, the validity of conventional effective medium theories (EMTs) tends to be inadequate and the effective permittivity of the metamaterial becomes dependent not only on the frequency of light, but also on its wavevector [22-24]. This becomes obvious in the epsilon-near-zero (ENZ) regime, where the contribution of spatial dispersion becomes increasingly important. The presence of these strong non-local terms drastically changes the optical properties of the material which leads to the appearance of an additional transverse or longitudinal wave [16].

The broad range of novel fundamental optical phenomena and prospective applications motivate this study of optical properties of wire materials. The rest of the thesis is organized as follows. First, a description of effective medium theory is presented along with a discussion of its applicability in describing wire based materials. Second, a computational and numerical study of the nonlocal optical response in plasmonic nanowire arrays is conducted and analyzed. This acts as the basis of comparison for all other numerical and analytical calculations to follow. Third, a complete investigation of the numerical results and a comparison with the current

models is conducted. Finally, an analytical technique that provides an adequate description of electromagnetism in wire-based metamaterials that takes into account nonlocal optical response originating from the homogenization procedure is obtained. This approach can be straightforwardly extended to describe optics of coaxial-cable-like media [25-27] and numerous other uniaxial composites.

2 Effective Medium Theory

We begin with one of the most common approaches in analyzing complex optical systems with subwavelength components. This is known as effective medium theory. In this technique, the properties of composite material are related to the optical properties of its constituents. The small (in comparison to wavelength) size of the components of the material makes it possible to solve Maxwell's equations in the quasistatic limit, where electric and magnetic responses of the system are decoupled from each other. The permittivity of (uniaxial) wire material and dispersion of the waves propagating in this medium are derived below.

2.1 Constitutive relationships in the quasistatic limit

We assume that the nanowire system operates in the effective-medium regime, which means that its inter-wire separation $a \ll \lambda_0$ with λ_0 being the free space wavelength. In addition, we follow the original work [28] and assume that surface concentration of wires is relatively small, $p = \pi R^2/a^2 \ll 1$, where R is the radius of the wire. The optical response of the nanowire materials resembles a uniaxial media with its optical axis in the direction of the wires. As such, the permittivity of metamaterial can be characterized by a diagonal tensor with components

$$\hat{\epsilon} = \begin{pmatrix} \epsilon_{x,y} & 0 & 0 \\ 0 & \epsilon_{x,y} & 0 \\ 0 & 0 & \epsilon_z \end{pmatrix} \qquad [2.1.1]$$

Using the Generalized Maxwell–Garnett formalism the boundary conditions of Maxwell's equations require that the E_z component be constant across the unit cell Fig. 2.1a. An individual wire excited by the homogeneous electric field in the *z*-direction may be written as

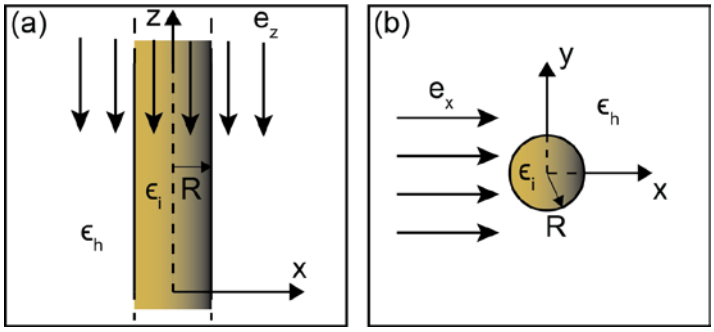

Figure 2.1: Dielectric wire in a constant external electric field (a) electric field in z-direction and (b) in-plane electric field in x-direction.

$$E_z^{mg} = \mathrm{e}_z^{mg} \qquad [2.1.2]$$

The in-plane components of the electric field (Fig. 2.1b) can be derived beginning with the solution of the Laplace equation for the potential. The general form of the potential for a homogeneous material in cylindrical coordinates is

$$\Phi = (A_0 + B_0 \ln r) + \sum_{m=1}^{\infty} (A_m r^m + B_m r^{-m})(C_m \cos(m\phi) + D_m \sin(m\phi)) \qquad [2.1.3]$$

Where the coefficients of linear expansion A_i, B_i, C_i and D_i are determined by the requirement that the potential is finite at $r = 0$, that the field away from the wire is converging to the field of the plane wave $\left[\Phi(r \gg R) = -\mathrm{e}_x^{mg} r \cos\phi\right]$, and by the boundary conditions requiring the continuity of $E_\tau(r = R)$ and $D_\perp(r = R)$. Therefore, inside the wire $r \leq R$

$$\Phi_i = A + \sum_{m=1}^{\infty} r^m (C_m \cos(m\phi) + D_m \sin(m\phi)) = A + rC_1 \cos\phi \qquad [2.1.4]$$

$$\vec{\boldsymbol{E}}_{\boldsymbol{i}} = -\nabla\Phi_i = -\frac{\partial\Phi_i}{\partial r}\hat{\boldsymbol{r}} - \frac{1}{r}\frac{\partial\Phi_i}{\partial\phi}\hat{\boldsymbol{\phi}} = C_1\left(-\cos\phi\,\hat{\boldsymbol{r}} + \sin\phi\,\hat{\boldsymbol{\phi}}\right) \quad [2.1.5]$$

while outside the wire $r \geq R$

$$\Phi_h = A + (A_1 r + B_1 r^{-1})\cos\phi \quad [2.1.6]$$

$$\vec{\boldsymbol{E}}_{\boldsymbol{h}} = -\left(A_1 - \frac{B_1}{r^2}\right)\cos\phi\,\hat{\boldsymbol{r}} + \frac{1}{r}\left(A_1 r + \frac{B_1}{r}\right)\sin\phi\,\hat{\boldsymbol{\phi}} \quad [2.1.7]$$

It is instructive to rewrite the expressions above in Cartesian coordinates,

$$\vec{\boldsymbol{E}}_{\boldsymbol{i}} = \frac{2\epsilon_h}{\epsilon_i + \epsilon_h}\mathrm{e}_x^{mg}\hat{\boldsymbol{x}} \quad [2.1.8]$$

$$\vec{\boldsymbol{E}}_{\boldsymbol{h}} = \mathrm{e}_x^{mg}\left[\left(1 + R^2\frac{\epsilon_h - \epsilon_i}{\epsilon_i + \epsilon_h}\frac{y^2 - x^2}{(x^2+y^2)^2}\right)\hat{\boldsymbol{x}} - \frac{2R^2xy}{(x^2+y^2)^2}\frac{\epsilon_h - \epsilon_i}{\epsilon_i + \epsilon_h}\hat{\boldsymbol{y}}\right] \quad [2.1.9]$$

Note that in the considered case of the excitation field is directed along the $\hat{x}$ axis, and the $\hat{y}$ component of the excited field is anti-symmetric with respect to x, y. Therefore, the only relevant component that does not vanish when averaged over the unit cell of the field becomes (see however, [30])

$$E_x^{mg} = \mathrm{e}_x^{mg} \times \begin{cases} \dfrac{2\epsilon_h}{\epsilon_i + \epsilon_h}, r \leq R \\ 1 + R^2\dfrac{\epsilon_h - \epsilon_i}{\epsilon_i + \epsilon_h}\dfrac{y^2 - x^2}{(x^2+y^2)^2}, r \geq R \end{cases} \quad [2.1.10]$$

Here ϵ_i and ϵ_h being the permitivitties of the wire inclusion and of the host material respectively, and the parameters $\mathrm{e}_z^{mg}$and e_x^{mg} are the field amplitudes. In the limit of small wire concentration,

interaction between the wires can be neglected. Taking the average of the fields over the unit cell for the j-th component yields the effective permittivity $\epsilon_j^{mg} = \langle \epsilon(x,y) E_j^{mg}(x,y) \rangle / \langle E_j^{mg}(x,y) \rangle$:

$$\epsilon_z^{mg} = \frac{\langle D_z^{mg} \rangle}{\langle E_z^{mg} \rangle} = \frac{p\epsilon_i \mathrm{e}_z^{mg} + (1-p)\epsilon_h \mathrm{e}_z^{mg}}{\mathrm{e}_z^{mg}} = p\epsilon_i + (1-p)\epsilon_h \qquad [2.1.11]$$

$$\epsilon_{x,y}^{mg} = \frac{\langle D_x^{mg} \rangle}{\langle E_x^{mg} \rangle} = \frac{p\epsilon_i \frac{2\epsilon_h}{\epsilon_i + \epsilon_h} \mathrm{e}_x^{mg} + (1-p)\epsilon_h \mathrm{e}_x^{mg}}{p\frac{2\epsilon_h}{\epsilon_i + \epsilon_h} \mathrm{e}_x^{mg} + (1-p)\mathrm{e}_x^{mg}} = \frac{2p\epsilon_i\epsilon_h + (1-p)\epsilon_h(\epsilon_i + \epsilon_h)}{2p\epsilon_h + (1-p)(\epsilon_i + \epsilon_h)} \qquad [2.1.12]$$

The derivations outlined above was originally considered in the context of the permittivity for nanosphere-based composites[28], often referred to as Maxwell Garnett formalism.

2.2 Dispersion Relationships

In this section let us derive the dispersion relationships governing light propagation in homogeneous uniaxial materials, and therefore governing the propagation of light in nanowire metamaterials in the limit of effective medium theory (EMT). We begin with Maxwell's equations

$$\nabla \cdot \vec{\boldsymbol{D}} = 4\pi\rho \qquad [2.2.1]$$

$$\nabla \cdot \vec{\boldsymbol{B}} = 0 \qquad [2.2.2]$$

$$\nabla \times \vec{\boldsymbol{E}} = -\frac{1}{c}\frac{\partial \vec{\boldsymbol{B}}}{\partial t} \qquad [2.2.3]$$

$$\nabla \times \vec{\boldsymbol{H}} = \frac{1}{c}\left(4\pi\vec{\boldsymbol{j}} + \frac{\partial \vec{\boldsymbol{D}}}{\partial t}\right) \qquad [2.2.4]$$

For an anisotropic composite the dielectric tensor must be diagonal and was shown in Eqn.(2.1.1). The propagating plane waves can be written as

$$\vec{\boldsymbol{E}} = \vec{\boldsymbol{E}}_0 \exp(i\vec{\boldsymbol{k}} \cdot \vec{\boldsymbol{r}} - i\omega t) \qquad [2.2.5]$$

$$\vec{\boldsymbol{H}} = \vec{\boldsymbol{H}}_0 \exp(i\vec{\boldsymbol{k}} \cdot \vec{\boldsymbol{r}} - i\omega t) \qquad [2.2.6]$$

By implementing Eqn.(2.2.1) with Eqn.(2.2.5) we get

$$\vec{\boldsymbol{k}} \cdot \hat{\epsilon}\vec{\boldsymbol{E}}_0 = 0 \qquad [2.2.7]$$

and Eqn.(2.2.3) with Eqns.(2.2.5) and (2.2.6) we can write the magnetic field in anisotropic non-magnetic medium as

$$\vec{\boldsymbol{H}}_0 = \frac{c}{\omega}\vec{\boldsymbol{k}} \times \vec{\boldsymbol{E}}_0 \qquad [2.2.8]$$

Finally Eqn.(2.2.4) on Eqn.(2.2.6) and the relation $\epsilon_o \mu_o c^2 = 1$ we obtain

$$\vec{\boldsymbol{k}} \times \vec{\boldsymbol{H}}_0 = -\frac{\omega}{c}\hat{\epsilon}\vec{\boldsymbol{E}}_0 = -\frac{\omega}{c}\vec{\boldsymbol{D}}_0 \qquad [2.2.9]$$

Eqns.(2.2.7) and (2.2.9) make up Maxwell's equations for a nonmagnetic anisotropic material.

Note that $\vec{\boldsymbol{D}} \perp \vec{\boldsymbol{k}}$, $\vec{\boldsymbol{D}} \perp \vec{\boldsymbol{H}}$, $\vec{\boldsymbol{H}} \perp \vec{\boldsymbol{E}}$, $\vec{\boldsymbol{H}} \perp \vec{\boldsymbol{k}}$. It was shown above that the vectors $\vec{\boldsymbol{D}}$ and $\vec{\boldsymbol{E}}$ are not necessarily co-aligned in anisotropic media, so $\vec{\boldsymbol{E}}$ and $\vec{\boldsymbol{k}}$ are not necessarily orthogonal to each other, see Fig. 2.2c.

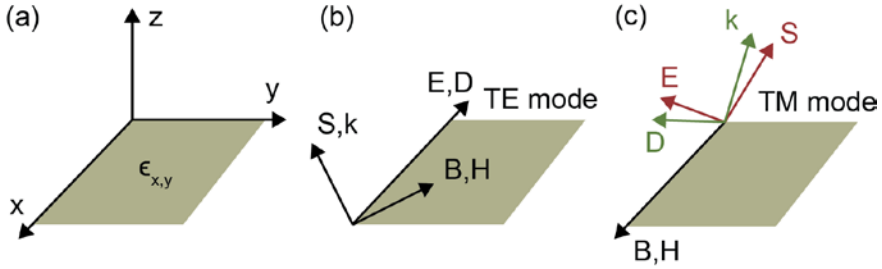

Figure 2.2: (b) TE-polarized ordinary waves are identical to isotropic systems. (c) TM-polarized extraordinary waves exhibit hyperbolic dispersion and have no diffraction limit when $\boldsymbol{\epsilon_{x,y}} \cdot \boldsymbol{\epsilon_z} < \mathbf{0}$.

One can obtain from Eqns.(2.2.8) and (2.2.9) the following relationship where any plane wave that satisfies Maxwell's equation must also satisfy the expression

$$k^2\vec{\boldsymbol{E}}_0 - \vec{\boldsymbol{k}}\left(\vec{\boldsymbol{k}} \cdot \vec{\boldsymbol{E}}_0\right) - \hat{\epsilon}\frac{\omega^2}{c^2}\vec{\boldsymbol{E}}_0 = 0 \qquad [2.2.10]$$

with $k^2 = \vec{\boldsymbol{k}} \cdot \vec{\boldsymbol{k}}$. In component form, where indices i, j correspond to Cartesian components, Eqn.(2.1.10) can be written as

$$\left(\delta_{ij}k^2 - k_i k_j - \epsilon_{ij}\frac{\omega^2}{c^2}\right)E_{0_i} = 0 \qquad [2.2.11]$$

In order for the electric field to have a non-zero amplitude the dispersion relation for a wave propagating in an anisotropic material reduces to the well-known expression

$$\left|\delta_{ij}k^2 - k_i k_j - \epsilon_{ij}\frac{\omega^2}{c^2}\right| = 0 \qquad [2.2.12]$$

with $\vec{\boldsymbol{k}}$ and ω being the wave vector and angular frequency of the plane wave, respectively, c being the speed of light in vacuum, ϵ is generally the nonlocal dielectric permittivity tensor of the metamaterial, and δ_{ij} is the Kroenecker delta symbol. When the permittivity does not depend on wavevector (also known as local regime) $\epsilon = \epsilon_{ij}^{mg}$. Expanding Eq.(2.2.12)

$$\begin{vmatrix} k_y^2 + k_x^2 - \epsilon_{x,y}^{mg}\frac{\omega^2}{c^2} & -k_x k_y & -k_x k_z \\ -k_x k_y & k_x^2 + k_z^2 - \epsilon_{x,y}^{mg}\frac{\omega^2}{c^2} & -k_y k_z \\ -k_x k_z & -k_y k_z & k_x^2 + k_y^2 - \epsilon_z^{mg}\frac{\omega^2}{c^2} \end{vmatrix} = 0 \qquad [2.2.13]$$

and solving for the dispersion allows two families of waves. One of these is known as ordinary, or transverse-electric wave, which is not affected by material anisotropy. While the second is

often called the extraordinary, or transverse-magnetic wave (see Fig. 2.2). The dispersion of these waves is characterized as:

$$k_x^2 + k_y^2 + k_z^2 = \epsilon_{x,y}^{mg} \frac{\omega^2}{c^2} \quad [2.2.14]$$

$$\frac{k_z^2}{\epsilon_{x,y}^{mg}} + \frac{k_x^2 + k_y^2}{\epsilon_z^{mg}} = \frac{\omega^2}{c^2} \quad [2.2.15]$$

By adjusting composition of the metamaterial and operating wavelength, the optical response of the composite can be controlled between all-dielectric elliptic ($\epsilon_{x,y}^{mg} > 0, \epsilon_z^{mg} > 0$) epsilon-near-zero (ENZ, $\epsilon_z^{mg} \approx 0$) and hyperbolic, which consists of ($\epsilon_{x,y}^{mg} > 0, \epsilon_z^{mg} < 0$) type I and ($\epsilon_{x,y}^{mg} < 0, \epsilon_z^{mg} > 0$) type II regimes. In the two latter regimes, metamaterial supports optical waves with either small or large effective modal index and motivate a number of potential applications in molding of light [31-33], cloaking [4,5], and subwavelength light manipulation[11-13,17].

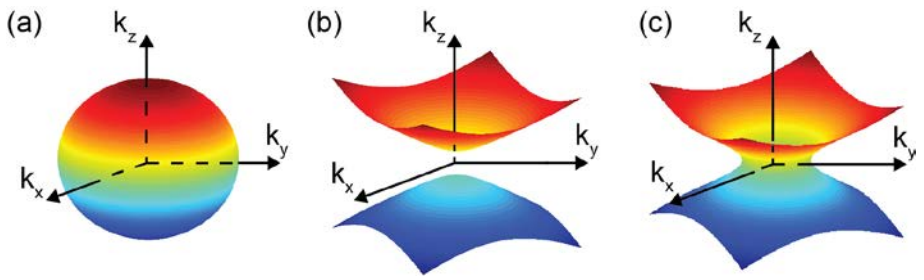

Figure 2.3: *k*-space topology. The dispersion for (a) and isoptropic dielectric is a sphere, and for (b) extraordinary waves in a uniaxial medium with extreme anisotropy it is a hyperboloid (type I). (c) Hyperboloid of a type II metamaterial.

To reiterate, a unique feature of hyperbolic metamaterials is evident from Fig. 2.3, which shows that the wavevector can exceed the free space wave vector ($k_0 = \omega/c$). Hyperbolic

metamaterials support a large number of electromagnetic states. An intuitive counting procedure in *k*-space consists of calculating the volume between the dispersion contours at $\omega(k)$ and $\omega(k) + \Delta\omega$. In a vacuum it is the equivalent to an infinitesimally thin spherical shell in *k*-space. For a hyperbolic metamaterial the dispersion modes have been shown to lie within the surface of a hyperboidal shell which has an infinite volume. In the effective medium limit this leads to a broadband singularity in the density of states [34]. There is no upper cut-off to the wave number in an ideal hyperbolic medium and an infinite number of *k* modes are supported. This phenomenon is the drive for further investigation and has vast potential in application for hyperbolic metamaterials.

2.3 Nonlocality

For most materials the dielectric permittivity tensor ϵ can be treated as a function of frequency alone. However, with the material sizes becoming smaller and smaller in length scales the finite wavelength of electrons can no longer be ignored. Following Landau and Lifshits [51] (see also [22, 35]), it is more correct and appropriate to use an approach based on taking spatial dispersion into account. An electric field in one place can produce a polarization in the near vicinity,

$$\vec{\boldsymbol{P}}(r) = \int \tilde{\chi}(r - r')\vec{\boldsymbol{E}}(r')dr' \qquad [2.3.1]$$

By converting Eq.(2.3.1) in reciprocal space we obtain the following form

$$\vec{\boldsymbol{P}}(\boldsymbol{k}) = \chi(\boldsymbol{k})\,\vec{\boldsymbol{E}}(\boldsymbol{k}) \qquad [2.3.2]$$

where polarizability (and, consequently, permittivity) depends on the wavevector $\boldsymbol{k}$. Note that if the material response is local $[\chi(r) \propto \delta(r - r')]$, permittivity in wavevector-domain does not

explicitly depend on k. In a majority of realistic materials nonlocality, if present, is weak, and thus it can be considered to be a correction to frequency-dependent response. If we take a Taylor expansion of $\epsilon(\boldsymbol{k})$, in centrosymmetic materials, the lowest non-vanishing term is proportional to k^2 .

$$\epsilon_{ij}(\boldsymbol{k}) = \epsilon_{ij}^{0}(\omega) + \sum_{l=1}^{3}\sum_{m=1}^{3} \alpha_{ijlm}(\omega) k_l k_m \qquad [2.3.3]$$

where α_{ijlm} is a 4th rank tensor.

The spatial dispersion appears in addition to the more familiar temporal, or frequency, dispersion, which is reflected in the dependence of the tensor on the frequency, ω. The spatial dispersion effects are usually much weaker than those arising from the frequency dispersion, but they can lead to qualitatively new phenomena, by substituting Eq. (2.3.3) into Eq. (2.2.12) an additional electromagnetic wave arises. These phenomena become increasingly important in the regime where permittivity of material approaches zero (often known as epsilon-near-zero, ENZ regime) since in this limit spatial dispersion, however small, dominates the material response.

Similar to homogeneous materials, it was shown that for nanowire meta-materials nonlocality needs to be taken into consideration at least in the ENZ regime[16]. Here the spatial dispersion changes the optical properties of the structure which leads to the excitation of an additional transverse-magnetic wave that is not described by local EMTs.

3 Numerical Calculations

For simplicity, the frequency of electromagnetic excitations and the unit cell parameters of the system are fixed and only the permittivity of the wire inclusions or substrate host are varied. The parameters primarily used throughout this work are $R = 20\,nm$, $a = 100\,nm$, $\epsilon_h = 1$, $L = 1\,\mu m$, $\lambda_0 = 1.5\mu m$ (see Fig. 3.1), which are typical for composites fabricated with anodized alumina templates [7,36]. Permittivity of the wire was varied between -10 and -3. This ensures that the parameters of the composite cover the important transition between elliptical response ($\epsilon_i \gtrsim -7$), epsilon-near-zero (ENZ) regime ($\epsilon_i \approx -7$), and hyperbolic response ($\epsilon_i \lesssim -7$) [see Fig.3.2].

Two separate numerical techniques for solving Maxwell's equations in periodic geometries were used, finite elements technique (FEM) and rigorous coupled wave analysis (RCWA).

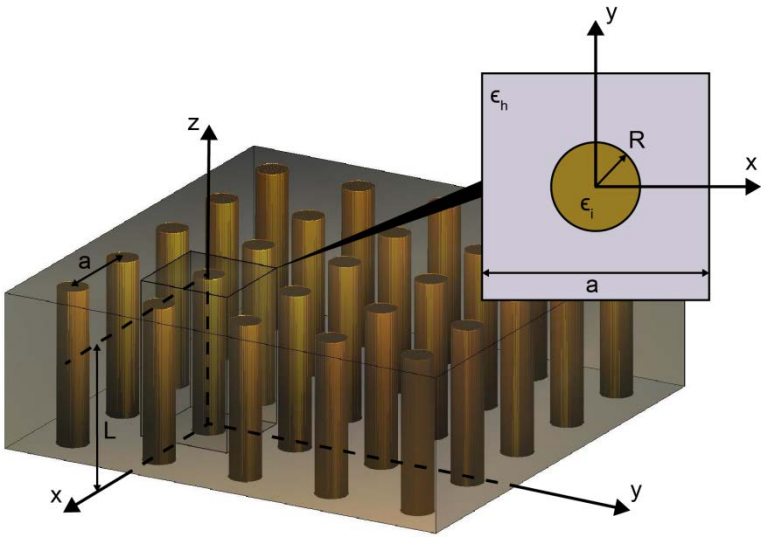

Figure 3.1: Schematic geometry and a unit cell of a nanowire composite.

First, a FEM solver [37] was used to perform numerical analysis of the eigenmodes of the periodic nanowire composites. A single unit cell was constructed as shown in (Fig. 3.1). To

mimic the response of the infinite periodic wire medium, we used Floquet periodicity for the boundary conditions.

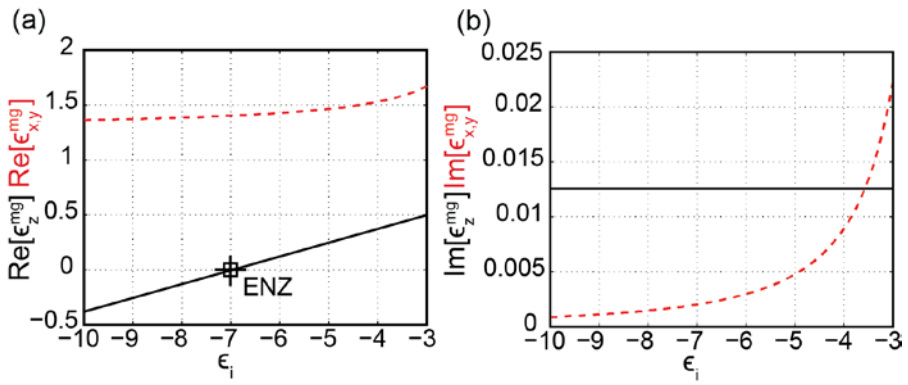

Figure 3.2: Permittivity derived from local EMT, $\epsilon_{x,y}^{mg}$ (dashed line) and ϵ_z^{mg} (solid line). The ENZ regime for the particular geometry under investigation is at $\epsilon_i \cong -7$ and illustrated by the cross in (a).

As with any periodic composite (photonic crystal), nanowire arrays support a large number of modes that essentially resemble the series of Bloch waves. It has been previously shown [16] that in the limit of small lattice size, depending on the material parameters, optical performance of nanowire composites is dominated by either two or three modes. The properties of one of these waves resemble the properties of TE-polarized mode in homogeneous composites, while the unit-cell-averaged polarization of the two other waves suggest their transverse-magnetic (TM)-polarized character, Fig. 3.3.

Due to the existence of multiple beams with identical polarization it is reasonable to assume that the behavior of the two average-TM-polarized waves in wire composites can be described by *nonlocal* (wavevector-dependent) effective medium theory. The goal of this thesis is to develop such a description.

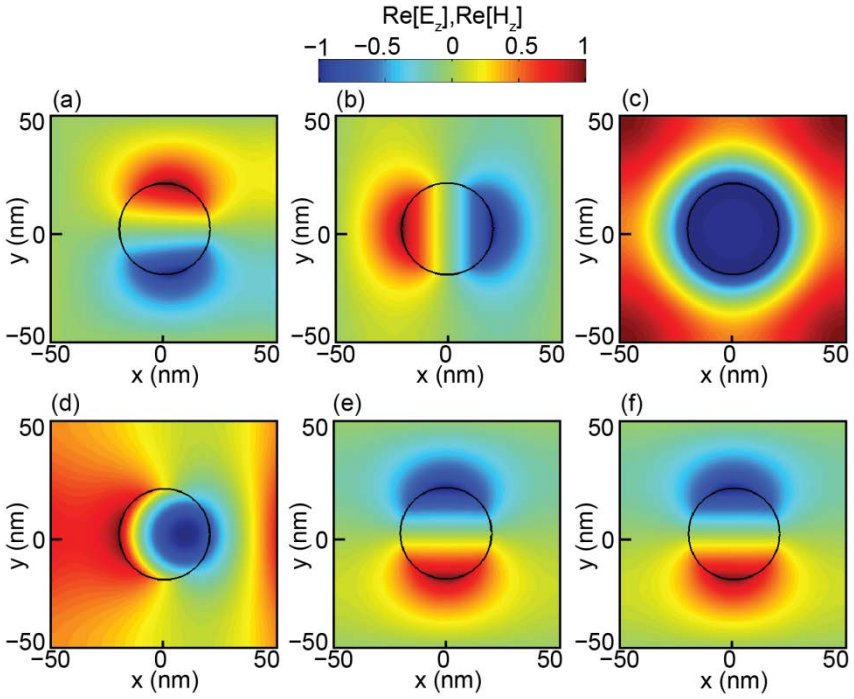

Figure 3.3: (a-c) Electric field and (d-f) Magnetic field profiles produced using FEM calculations. (a,d) Represents the TE-mode, (b,e) the TM or extraordinary -mode and (c,f) the additional TM-mode which has been predicted and observed in previous experimental results.

In this model, the two TM waves identified in the numerical simulations represent the main and additional TM waves that are supported by the nanowire metamaterial. The main wave has a relatively smooth E_z profile (Fig. 3.3 b,e) in comparison to the additional wave which has strong non-uniform field profile (Fig. 3.3 c,f).

3.1 Two Dimensional Rigorous Coupled Wave Analysis (2DRCWA)

To provide independent verification of FEM-based solutions of Maxwell equations, the 2D analog of RCWA [38] is developed and implemented. In this formalism, that takes advantage of 2D periodicity of material permittivity, the latter is represented using 2D discrete Fourier transform:

$$\epsilon(x,y) = \sum_{m,n} \epsilon_{mn} e^{-i(mq_x x + nq_y y)} \qquad [3.1.1]$$

where $q_\alpha = \frac{2\pi}{\mathrm{a}_\alpha}$ plays the role of the Bloch-vector, and subscript α defines the in-plane coordinate (*x* or *y)*. Using the Bloch theorem, we represent the fields in the unit cell by

$$\boldsymbol{E}, \boldsymbol{H} = \sum_{m,n} (\boldsymbol{e}, \boldsymbol{h})_{m,n} e^{i\boldsymbol{k}^{m,n}\cdot\boldsymbol{r} - i\omega t} \qquad [3.1.2]$$

with

$$\boldsymbol{k}^{m,n} = (k_x + mq_x)\hat{x} + \left(k_y + nq_y\right)\hat{y} + k_z\hat{z} \qquad [3.1.3]$$

Explicit substitutions of Eqs.(3.1.1 and 3.1.3) into Eq.(2.2.12), yields the dispersion relation

$$\boldsymbol{k}^{m,n}\left(\boldsymbol{k}^{m,n}\cdot\boldsymbol{e}_{m,n}\right) - \sum_{\alpha,\beta} \boldsymbol{e}_{\boldsymbol{\alpha},\beta}\left[\left|\boldsymbol{k}^{\alpha,\beta}\right|^2 \delta_{\alpha-m,\beta-n} - \frac{\omega^2}{c^2}\epsilon_{\alpha-m,\beta-n}\right] = 0 \qquad [3.3.4]$$

Replacing $(m,n) \to \xi$ and $(\alpha,\beta) \to \eta$ transforms the $m \times n$ and $\alpha \times \beta$ matrices into a diagonal matrix, where the indices ξ and η are one-dimensional indices that now span two-dimensional space. With this transformation and the use of Maxwell's equations we obtain

$$\boldsymbol{k}^{\xi} \times \boldsymbol{h}_{\xi} = -\frac{\omega}{c}\boldsymbol{e}_{\eta}\hat{\epsilon}_{\eta-\xi} \qquad [3.3.5]$$

$$\boldsymbol{k}^{\xi} \times \boldsymbol{e}_{\xi} = \frac{\omega}{c}\boldsymbol{h}_{\xi} \qquad [3.3.6]$$

The Eqns.(3.3.5) and (3.3.6) now form a basis where the eigenvalue k_z and eigenvectors $\boldsymbol{e}, \boldsymbol{h}$ for each mode can be solved. The FEM simulations and 2D RCWA yield comparable results (Fig. 3.4).

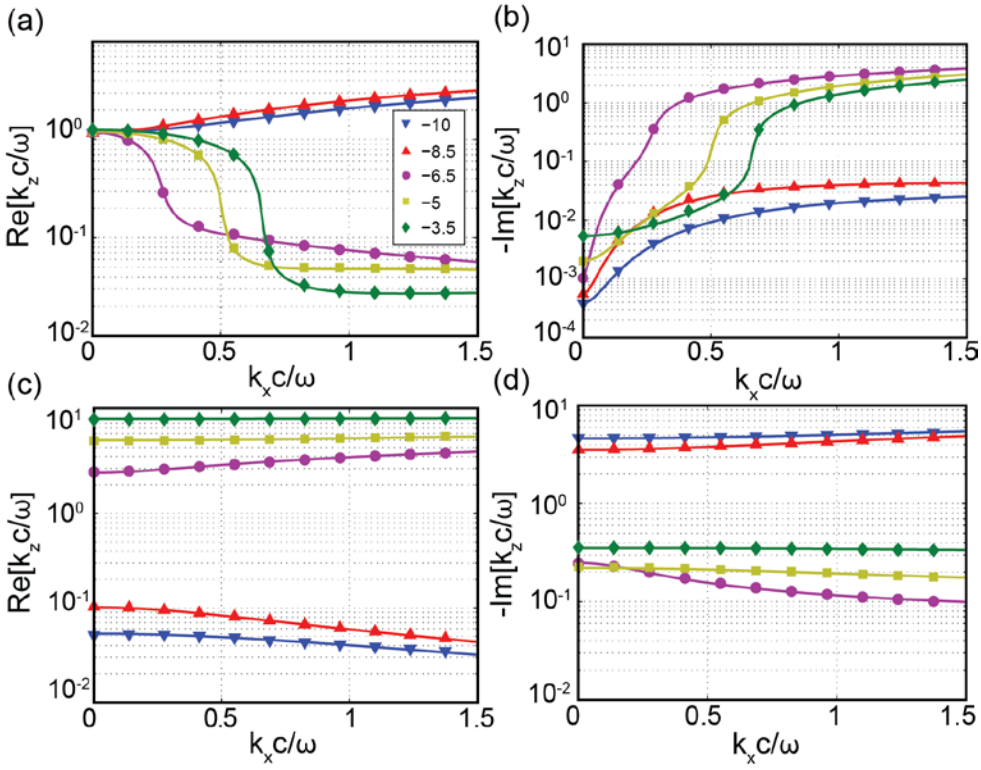

Figure 3.4 Dispersion of the modes guided by the nanowire metamaterial, calculated with full-wave solutions of Maxwell equations (lines) and 2DRCWA (symbols)

3.2 Comparison of Numerical Results with EMT

To first explore the validity and applicability of EMTs the dispersion of the TE-polarized and TM-polarized waves are extracted from numerical calculations and compared with the dispersion predicted by Eqs.(2.2.14) and (2.2.15). One way that the parameter $\epsilon_{x,y}$ and ϵ_z can be determined numerically is by minimizing the mean-square deviation,

$$\Delta = \sum_i \left| \tilde{k}_{zi}^2 - k_z^2 \right|^2 \rightarrow min. \qquad [3.2.1]$$

where k_z is calculated using Eq.(2.2.14) or (2.2.15), while $\tilde{k}_{zi}$ is taken from the numerical solutions to Maxwell's equations (Fig. 3.4). Eqn.(3.2.1) can be solved analytically from the TE-polarized wave yielding

$$\epsilon_{x,y}^{LS} = \frac{c^2}{\omega^2 N} \sum_{i=1}^{N} \tilde{k}_{z_i}^2 + {k_x}_i^2 \qquad [3.2.2]$$

Similarly, the parameter ϵ_z can be determined by minimizing the deviation of calculated dispersion of main TM-polarized wave from its expected elliptical (or hyperbolic) behavior. This procedure yields

$$\epsilon_z^{LS} = \sum_{i=1}^{N} \frac{k_{x_i}^2}{\epsilon_{x,y}^{LS} \frac{\omega^2}{c^2} - \tilde{k}_{z_i}^2} \qquad [3.2.3]$$

Once the effective permittivity is fit to the numerical solutions of Maxwell's equations, a comparison can be made to the analytical predictions of EMT. This comparison between the mean-square deviation and analytical effective medium parameters is shown in Fig.3.5. It is seen that $\epsilon_{x,y}$ is adequately described by Eq. (2.1.12). However, Eq. (2.1.11) deviates from the fit value and this deviation is particularly strong at the ENZ ($\epsilon_z \rightarrow 0$) regime. In particular, numerically-derived ϵ_z seems to depend on the k_x component of permittivity; with Eq.(2.1.11) less accurately describing optics of nanowire systems for larger values of k_x. This is validated

by reducing the limit of the maximum k_x term used in the summation to determine the numerical permittivities, Eqs.(3.2.2) and (3.2.3). As this term is reduced it can be seen from Fig. 3.5 that the permittivity ϵ_z (triangles) is now in better agreement with EMT (solid line).

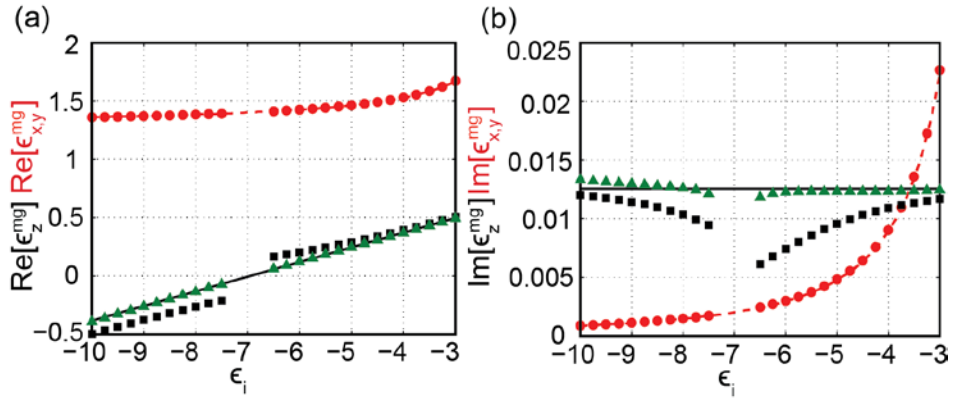

Figure 3.5 Permittivity derived from local EMT (lines) compared with the permittivity calculated using least square approximation (symbols) eqns. 3.2.2 and 3.2.3. The transverse permittivity is in good agreement for all values of k_x however the permittivity parallel to the wires is not especially near ENZ (squares). The agreement improves for smaller maximum value of k_x (triangles).

When ϵ_z is sufficiently different from zero, however, there seems to be reasonable agreement between the predictions of local EMT [6,30,39,40] and properties of the main TM-polarized wave in wire composites, in particular in the limit of relatively small k_x (Figs. 3.5-3.7).

To further investigate the relationship between the numerical and the local dispersion, Eqs.(2.1.11) and (2.1.12), are plotted. It can be seen from Fig. 3.6 that the local theories inadequately describe the dispersion relationship for the transverse-magnetic polarized wave. Finally the numerical permittivity obtained by averaging the wave profiles from the FEM results and the analytical EMT permittivity as a function of k_x are compared. Here (Fig. 3.7) the deviation at large values of k_x become obvious for the TM-mode.

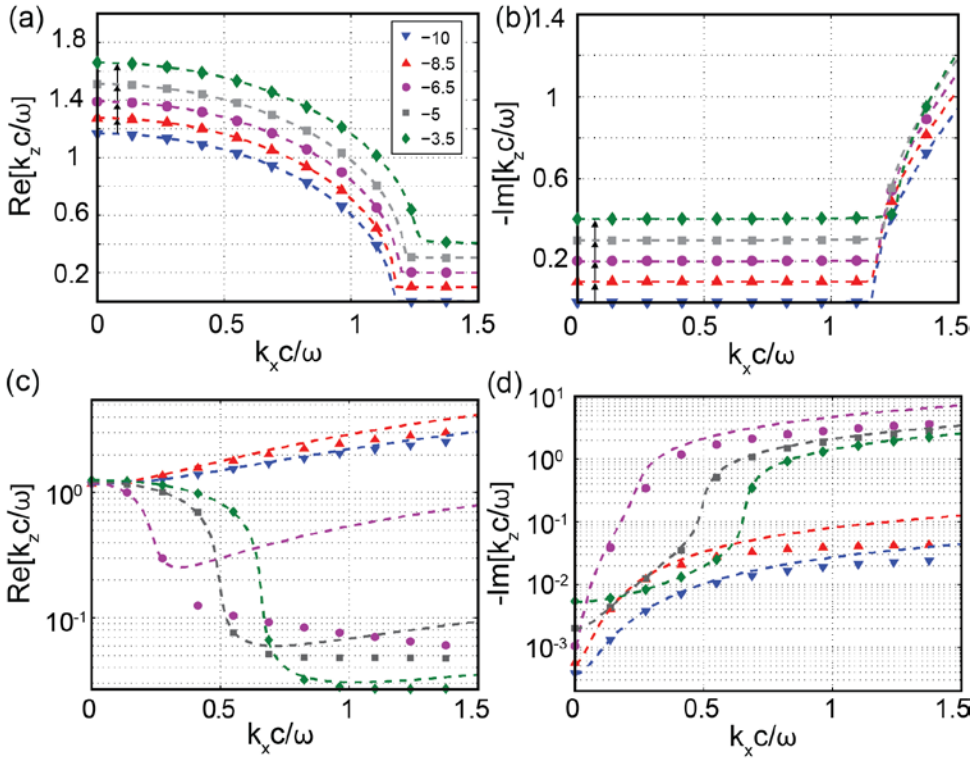

Figure 3.6 A comparison between local EMT dispersion (dashed lines) and FEM calculations. (symbols). (a,b) TE-mode comparison which is in good agreements (note the axis is shifted by 0.1 to show distinction between each dispersion curve). (c,d) TM-mode comparison, here it can be clearly shown that there is a deviation for large values of k_x.

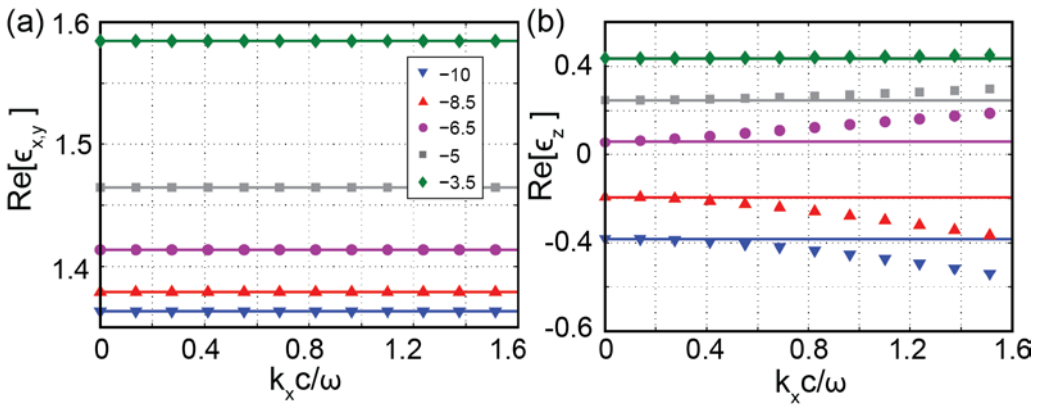

Figure 3.7 A comparison between local EMT permittivity (lines) and FEM calculations. (symbols). (a) TE-mode comparison which is in good agreements. (b) TM-mode comparison, here it can be clearly shown that there is a deviation for large values of k_x.

To summarize, local effective medium theory falls short in several major areas. First, it fails to accurately describe the fundamental optical properties for uniaxial materials at relatively large (in comparison with ω/c) values of k_x, and near the ENZ regime. Second, and more importantly, it does not predict the additional TM-mode. In the next sections we summarize previous attempts to develop nonlocal effective medium theories that attempt to describe optical properties of wire composites.

3.3 Comparison with earlier nonlocal effective medium theories

The problem of light interaction with nonlocal wire media has been considered before. A realistic wire composite in the effective medium regime supports three electromagnetic modes. With few exceptions, the majority of the studies that focus on high-frequency response of wire composites [6,30,39-41] predict a single extraordinary and a single ordinary wave at every frequency. Most of the studies that do predict the existence of additional electromagnetic waves [24,42,43] have focused on optics for highly conductive (PEC-like) wires. Refs. [24,42,43] presents an attempt to generalize the developed formalism to the case of plasmonic media. Figs. 3.8 and 3.9 present a comparison of the formalism from [24,43] and full wave numerical solutions of Maxwell's equations.

Fig. 3.8 clearly demonstrates that the approach developed in [24,43] severely underestimates the effective modal index of the waves propagating in plasmonic wire media (similar phenomenon can also be seen in Fig. 3 of [24]). This under-estimation yields significant errors in calculations of optical properties of wire composites, seen in Fig. 5 of [43] that can be only be eliminated by using a heuristic "correction factor".

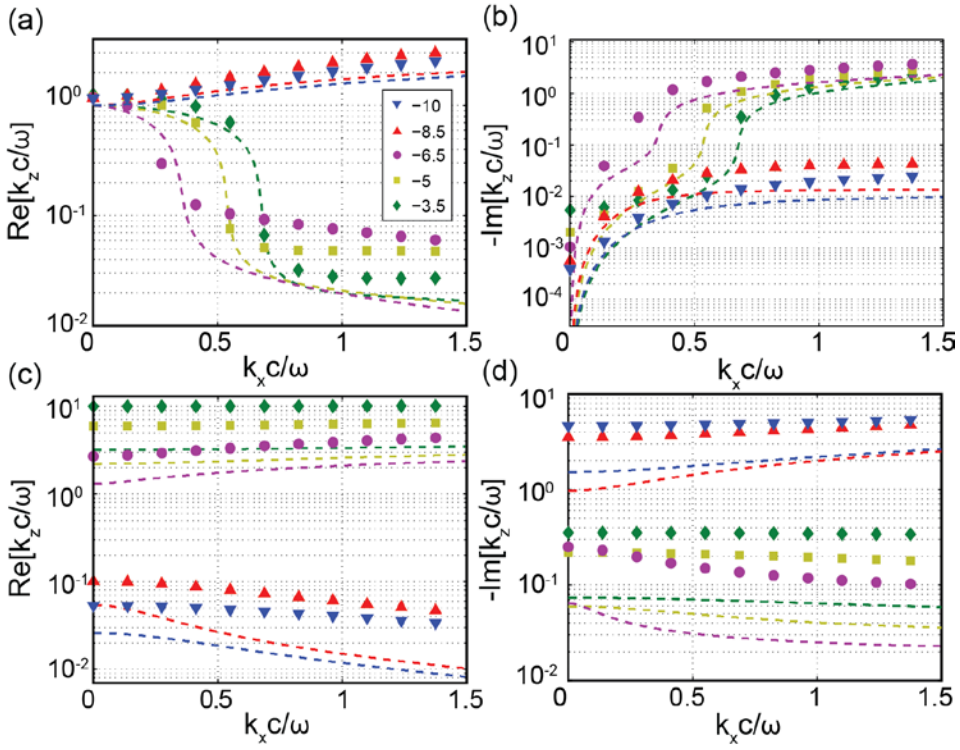

Figure 3.8: Dispersion of the modes guided by the nanowire metamaterial, calculated with full-wave solutions of Maxwell equations (symbols) with earlier approach, designed for highly-conducting wires [24,43] (dashed lines)

The [24,43] model and numerical effective permittivity for increasing k_x is also shown to have significant errors. As k_x increases the variation becomes dramatic and the need for a more accurate model could not be more evident.

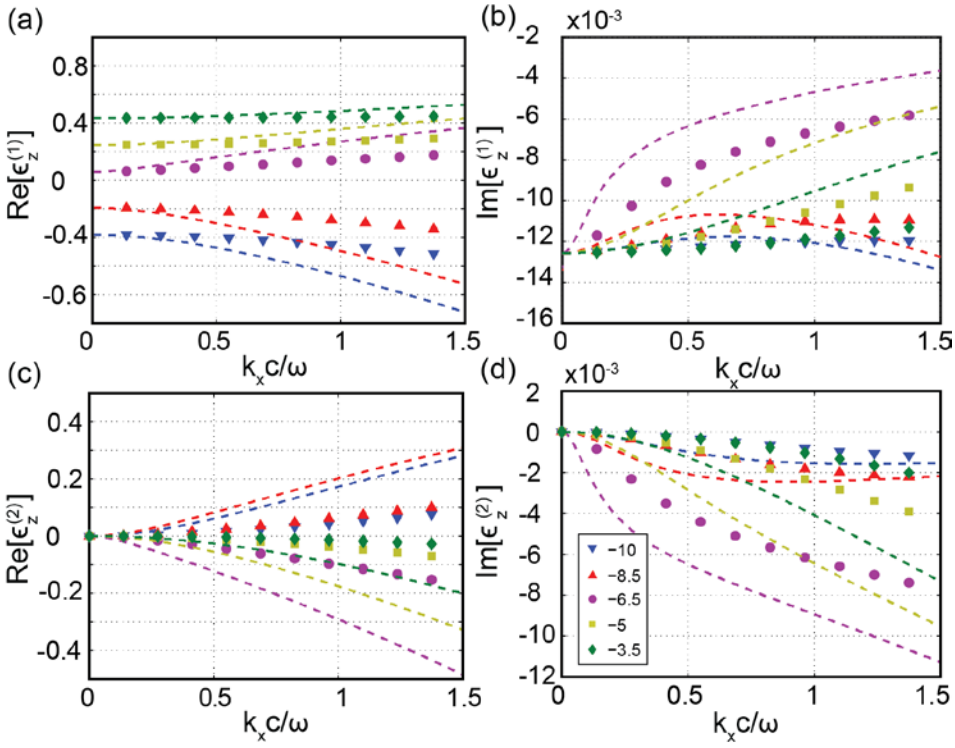

Figure 3.9: Effective permittivity defined as $\epsilon_z = \langle \epsilon(x,y) E_z(x,y) \rangle / \langle E_z(x,y) \rangle$, calculated with full-wave solutions of Maxwell equations (symbols) with earlier approach, designed for highly-conducting wires [24,43] (dashed lines).

4 Beyond Effective Medium Theory: Perturbation approach

One major problem is that the deviation of dispersion of the main TM-polarized mode in wire composites from the predictions of local EMT becomes much stronger in the ENZ regime. This behavior is qualitatively similar to behavior predicted (and later observed at ultra-low temperatures [22,23,44]) in nonlocal (permittivity dependent on wavevector) homogeneous materials. Quantitatively, (weak) dependence of effective permittivity on wavevector can be considered with a perturbation-type correction to frequency-dependent permittivity, given by

$$\epsilon_z \cong \epsilon_z(\omega) + \alpha_z \frac{k_z^2 c^2}{\omega^2} \qquad [4.1]$$

with $|\alpha_z| \ll 1$.

The nonlocality of the *z* component of the permittivity only affects propagation of the TM-polarized mode. This wavevector-dependent term changes the response of the system thus enabling a new kind of plane wave, known as the additional wave. By substituting Eq. (4.1) into (2.2.13) a modified dispersion relationship can be derived that takes into account this correction, and is given by

$$2\alpha_z k_z^2 = (\epsilon_z + \xi)\frac{\omega^2}{c^2} \pm \frac{\omega}{c}\sqrt{(\epsilon_z - \xi)^2 \frac{\omega^2}{c^2} + 4\xi {k_x}^2} \qquad [4.2]$$

where $\xi = \alpha_z \epsilon_{x,y}^{mg}$

In the limiting case where $\alpha_z \to 0$, one of the roots converges to Eq. (2.2.15) while the other root goes to infinity. Therefore, the additional wave is always present in nonlocal

metamaterials, but the large index mismatch may prevent its coupling with free plane waves. The ratio between the parameter α_z and the minimal value of $\epsilon_z(\omega)$ is the effectiveness of coupling incident light into the additional wave. Excitation of the additional wave at ENZ in response of wire composites has been experimentally demonstrated, at room temperature, in [16].

The fitting procedure that was developed in Section 3.2 is implemented to extract the parameters of perturbation-based nonlocal dispersion relation, Eq. (4.2). Note that the least square fitting procedure becomes nonlinear; therefore, empirical solutions for the four parameters, $\Re e(\epsilon_z)$, $\Im m(\epsilon_z)$, $\Re e(\alpha_z)$, and $\Im m(\alpha_z)$, cannot be determined. Instead numerical values of these four parameters were simultaneously determined by nonlinear least square fit optimization[45-50].

After a solution for the parameters are determined the nonlocal dispersion can be calculated and compared with the numerical solutions from Maxwell's equations Fig. 4.1. It can be seen in the figure below that this technique appears to predict both waves and describes the dispersion with excellent accuracy.

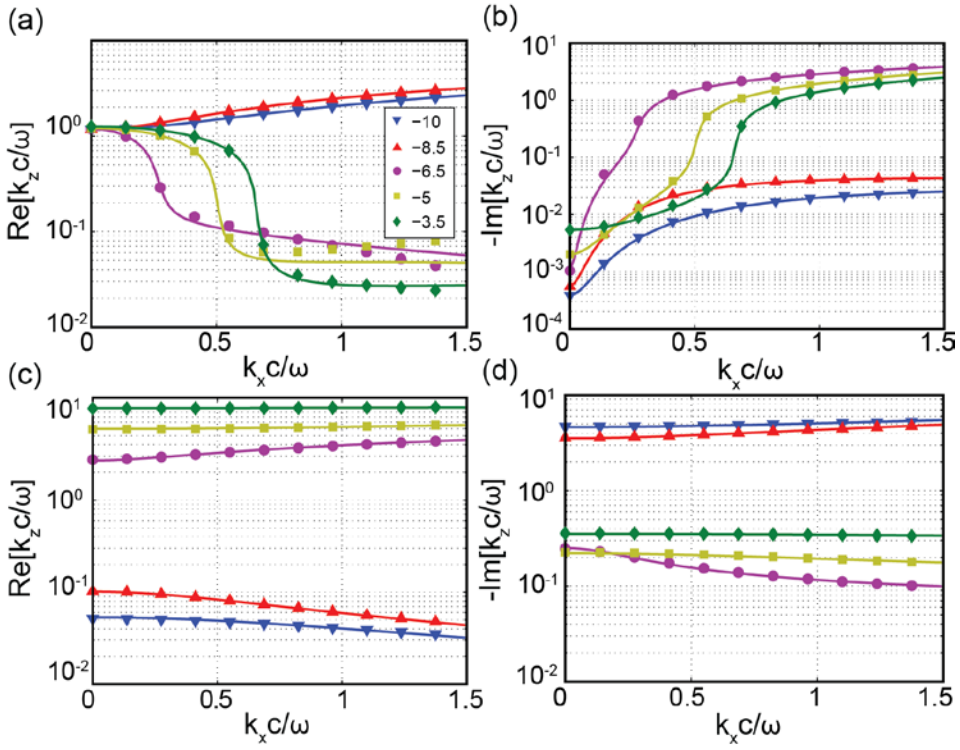

Figure 4.1: Dispersion of the modes guided by the nanowire metamaterial, calculated with full-wave solutions of Maxwell equations (symbols) with nonlocal dispersion approach (lines).

However, further analysis reveals that the nonlocality parameter α_z, as determined by nonlinear optimization procedure, is mode-dependent (Fig. 4.2), i.e. it has different values for main and additional TM-polarized modes. Thus, it is obvious that perturbative technique Eq. (4.2) does not provide an adequate description of optical properties of plasmonic wire arrays.

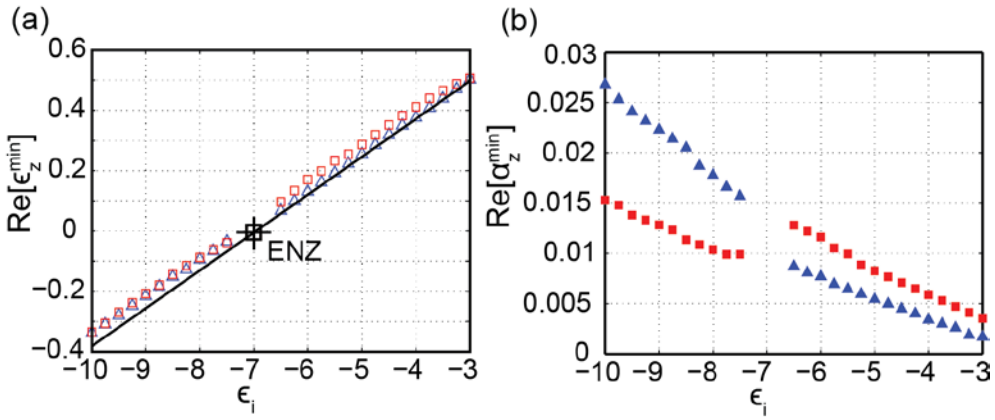

Figure 4.2: (a) Comparison between ϵ_z^{mg} (line) and ϵ_z^{min} (symbols). The triangles represent the TM or extraordinary mode and squares the additional TM-mode. (b) The nonlocal fitting parameter α_z^{min} (symbols) for varying ϵ_i, here the mode dependency can be clearly seen.

5 Analytical Description of the Nonlocal Optical Response

In this section an analytical description for the optical properties of nonlocal nanowire systems is presented. First, light propagation in the direction of the wire is considered and the propagation constants of the two TM-polarized waves that are supported by the composite are identified in this regime. Lastly, it is shown how to calculate the dispersion and wave profiles for off angle light propagation and compare these results with numerical calculations.

The electromagnetic field within the unit cell (Fig. 3.1) can be derived from first principles. Within the nanowire material there are no free charges and Maxwell's equations are used to obtain the generalized wave equation

$$\nabla^2\vec{\mathrm{F}} - \frac{\epsilon\mu}{c^2}\frac{\partial^2\vec{\mathrm{F}}}{\partial t^2} = 0. \qquad [5.1]$$

where $\vec{\mathrm{F}} = \vec{\mathrm{E}}, \vec{\mathrm{H}}$. Since the nanowire material is nonmagnetic, without loss of generality, we can set the permeability to unity. The wave equation then reduces to the following form

$$\nabla^2\vec{\mathrm{F}} - \frac{\epsilon}{c^2}\frac{\partial^2\vec{\mathrm{F}}}{\partial t^2} = 0. \qquad [5.2]$$

It can be shown (see below) that for a wave propagating along the z direction, all the transverse components of $\vec{\mathrm{F}}$ can be expressed in terms of the longitudinal component F_z [51]. In Cylindrical coordinates the differential equation for this remaining component takes the form

$$\nabla^2 F_z - k^2 F_z = \left(\frac{1}{r}\frac{\partial}{\partial r}\left(r\frac{\partial}{\partial r}\right) + \frac{1}{r^2}\frac{\partial^2}{\partial \phi^2} + \frac{\partial^2}{\partial z^2}\right)F_z - k^2 F_z = 0, \qquad [5.3]$$

where $k^2 = \epsilon\omega^2/c^2$. The solution can be expressed as the product $F_z = R(r)P(\phi)Z(z)$. Making this substitution, the differential equation can then be written as

$$\frac{1}{rR}\frac{d}{dr}\left(r\frac{dR}{dr}\right) + \frac{1}{r^2P}\frac{d^2P}{d\phi^2} + \frac{1}{Z}\frac{d^2Z}{dz^2} + k^2 = 0\,. \qquad [5.4]$$

From the above equation we arrive at the solution $Z(z) = z_o e^{ik_z z}$, and if we multiply through by r^2 we are left with

$$\frac{r}{R}\frac{d}{dr}\left(r\frac{dR}{dr}\right) + \frac{1}{P}\frac{d^2P}{d\phi^2} + (k^2 - k_z^2)r^2 = 0. \qquad [5.5]$$

Notice that the equation is now completely separable by variables. Let's first solve for *P*,

$$\frac{1}{P}\frac{d^2P}{d\phi^2} = \lambda^2 = const. \qquad [5.6]$$

we can choose $\lambda^2 = -m^2$ with *m* = 0,1,2,.. leading to

$$P(\phi) = A\sin(m\phi) + B\cos(m\phi). \qquad [5.7]$$

The differential equation can now be written in terms of only the variable *r*

$$\frac{r}{R}\frac{d}{dr}\left(r\frac{dR}{dr}\right) - m^2 + (k^2 - k_z^2)r^2 = r^2\frac{d^2R}{dr^2} + r\frac{dR}{dr} + [(k^2 - k_z^2)r^2 - m^2]R = 0 \qquad [5.8]$$

Let's first choose $\kappa = \sqrt{\epsilon\omega^2/c^2 - k_z^2}$ so the equation becomes

$$r^2 \frac{d^2R}{dr^2} + r \frac{dR}{dr} + [\kappa^2 r^2 - m^2]R = 0. \quad [5.9]$$

The solution to the above differential equation is the well-known Bessel function

$$R(r) = c_1 J_m(\kappa r) + c_2 Y_m(\kappa r). \quad [5.10]$$

The final solution can be written as

$$F_z(r, \phi, z) = \sum_m \big(c_{1m} J_m(\kappa r) + c_{2m} Y_m(\kappa r)\big) \sin(m\phi)\, e^{ik_z z} + \big(c_{3m} J_m(\kappa r) + c_{4m} Y_m(\kappa r)\big) \cos(m\phi)\, e^{ik_z z} \quad [5.11]$$

Here boundary conditions must be applied to solve for the amplitudes of the individual cylindrical waves.

5.1 Calculation of E_z and H_z

The nanowire metamaterial can be separated into two regions, (i) inside and (ii) outside the wire material. An expression for the fields will be derived for both by applying initial boundary conditions to the generalized field expression previously obtained (Eq. 5.11).

Inside the nanowire

First we will look at the solution inside the wire, we can write $\kappa_i = \sqrt{\epsilon_i \omega^2/c^2 - k_z^2}$ and as $r \to 0$, $Y_m(\kappa_i r) \to \infty$ thus c_{2m} and $c_{4m} = 0$. Due to the symmetric nature of the problem it is satisfactory to examine the fields at just $z = 0$,

$$F_z^i = \sum_m J_m(\kappa_{in} r)(A_m^i \sin(m\phi) + B_m^i \cos(m\phi)) \quad [5.1.1]$$

and $E_z^l \propto \cos(m\phi)$ and $H_z^l \propto \sin(m\phi)$, using these results the inner wire field equations can be written as

$$E_z^l(r \leq R) = \sum_m a_m J_m(\kappa_{in} r) \cos(m\phi) \quad [5.1.2]$$

$$H_z^l(r \leq R) = \sum_m b_m J_m(\kappa_{in} r) \sin(m\phi) \quad [5.1.3]$$

Outside the nanowire

Outside the wire the second order Bessel function does not vanish. We can express this result in terms of Hankel functions, where $\kappa_h = \sqrt{\epsilon_h \omega^2/c^2 - k_z^2}$

$$F_z^h = \sum_m (c_{1m}^h H_m^+(\kappa_h r) + c_{2m}^h H_m^-(\kappa_h r))(A_m^h \sin(m\phi) + B_m^h \cos(m\phi)) \quad [5.1.4]$$

where $H_m^+ = J_m + iY_m$ and $H_m^- = J_m - iY_m$. The outer wire fields can be written as

$$E_z^l(r > R) = \sum_m (\alpha_m^+ H_m^+(\kappa_h r) + \alpha_m^- H_m^-(\kappa_h r)) \cos(m\phi) \quad [5.1.5]$$

$$H_z^l(r > R) = \sum_m (\beta_m^+ H_m^+(\kappa_h r) + \beta_m^- H_m^-(\kappa_h r)) \sin(m\phi) \quad [5.1.6]$$

5.2 Calculation of E_r, H_r, E_ϕ, and H_ϕ

To obtain the fields in the other two directions we must begin with Maxwell's equations $\nabla \times \boldsymbol{E} = -\frac{1}{c}\frac{\partial \boldsymbol{H}}{\partial t}$ and $\nabla \times \boldsymbol{H} = \frac{\epsilon}{c}\frac{\partial \boldsymbol{E}}{\partial t}$. Using the identity $\nabla \times \boldsymbol{A} = \hat{r}\left(\frac{1}{r}\frac{\partial A_z}{\partial \phi} - \frac{\partial A_\phi}{\partial z}\right) + \hat{\phi}\left(\frac{\partial A_r}{\partial z} - \frac{\partial A_z}{\partial r}\right) + \hat{z}\left(\frac{1}{r}\frac{\partial}{\partial r}(rA_\phi) - \frac{1}{r}\frac{\partial A_r}{\partial \phi}\right)$ we can write down the following relationships

$$\frac{\partial E_r}{\partial t} = \frac{c}{\epsilon}\left(\frac{1}{r}\frac{\partial H_z}{\partial \phi} - \frac{\partial H_\phi}{\partial z}\right) \quad [5.2.1] \qquad \frac{\partial H_r}{\partial t} = c\left(\frac{\partial E_\phi}{\partial z} - \frac{1}{r}\frac{\partial E_z}{\partial \phi}\right) \quad [5.2.2]$$

$$\frac{\partial E_\phi}{\partial t} = \frac{c}{\epsilon}\left(\frac{\partial H_r}{\partial z} - \frac{\partial H_z}{\partial r}\right) \quad [5.2.3] \qquad \frac{\partial H_\phi}{\partial t} = c\left(\frac{\partial E_z}{\partial r} - \frac{\partial E_r}{\partial z}\right) \quad [5.2.4]$$

$$\frac{\partial E_z}{\partial t} = \frac{c}{\epsilon}\left(\frac{1}{r}\frac{\partial}{\partial r}(rH_\phi) - \frac{1}{r}\frac{\partial H_r}{\partial \phi}\right) \quad [5.2.5] \qquad \frac{\partial H_z}{\partial t} = c\left(\frac{1}{r}\frac{\partial E_r}{\partial \phi} - \frac{1}{r}\frac{\partial}{\partial r}(rE_\phi)\right) \quad [5.2.6]$$

The fields can generally be written as

$$\boldsymbol{E} = \boldsymbol{E}_o e^{ik_z z - i\omega t} \rightarrow \begin{cases} E_r e^{ik_z z - i\omega t} \\ E_\phi e^{ik_z z - i\omega t} \\ E_z e^{ik_z z - i\omega t} \end{cases} \quad [5.2.7] \qquad \boldsymbol{H} = \boldsymbol{H}_o e^{ik_z z - i\omega t} \rightarrow \begin{cases} H_r e^{ik_z z - i\omega t} \\ H_\phi e^{ik_z z - i\omega t} \\ H_z e^{ik_z z - i\omega t} \end{cases} \quad [5.2.8]$$

After making the appropriate substitutions and some algebra we arrive at the following results

$$E_r = \frac{i}{\kappa^2}\left(k_z \frac{\partial E_z}{\partial r} + \frac{\omega}{rc}\frac{\partial H_z}{\partial \phi}\right) \rightarrow \begin{cases} E_r^{TE} = \dfrac{i\omega}{r\kappa^2 c}\dfrac{\partial H_z}{\partial \phi} \\ E_r^{TM} = \dfrac{ik_z}{\kappa^2}\dfrac{\partial E_z}{\partial r} \end{cases} \quad [5.2.9]$$

$$H_r = \frac{i}{\kappa^2}\left(-\frac{\epsilon\omega}{rc}\frac{\partial E_z}{\partial\phi} + k_z\frac{\partial H_z}{\partial r}\right) \rightarrow \begin{cases} H_r^{TE} = \dfrac{ik_z}{\kappa^2}\dfrac{\partial H_z}{\partial r} \\ H_r^{TM} = -\dfrac{i\epsilon\omega}{r\kappa^2 c}\dfrac{\partial E_z}{\partial\phi} \end{cases} \quad [5.2.10]$$

$$E_\phi = \frac{i}{\kappa^2}\left(\frac{k_z}{r}\frac{\partial E_z}{\partial\phi} - \frac{\omega}{c}\frac{\partial H_z}{\partial r}\right) \rightarrow \begin{cases} E_\phi^{TE} = -\dfrac{i\omega}{\kappa^2 c}\dfrac{\partial H_z}{\partial r} \\ E_\phi^{TM} = \dfrac{ik_z}{r\kappa^2}\dfrac{\partial E_z}{\partial\phi} \end{cases} \quad [5.2.11]$$

$$H_\phi = \frac{i}{\kappa^2}\left(\frac{\epsilon\omega}{c}\frac{\partial E_z}{\partial r} + \frac{k_z}{r}\frac{\partial H_z}{\partial\phi}\right) \rightarrow \begin{cases} H_\phi^{TE} = \dfrac{ik_z}{r\kappa^2}\dfrac{\partial H_z}{\partial\phi} \\ H_\phi^{TM} = \dfrac{i\epsilon\omega}{\kappa^2 c}\dfrac{\partial E_z}{\partial r} \end{cases} \quad [5.2.12]$$

Using these equations and our expression for $E_z \rightarrow E_z^l$ and $H_z \rightarrow H_z^l$ we can now write the fields in the $r-$ direction and $\phi-$ direction, let's note that all $J_m(\kappa_i r) \rightarrow J_m$ and $H_m^{+/-}(\kappa_h r) \rightarrow H_m^{+/-}$ for simplicity

$$E_r^l(r \le R) = \frac{ik_z^l}{\kappa_i}\sum_m a_m J'_m \cos(m\phi) + \frac{i\omega}{r\kappa_i^2 c}\sum_m m b_m J_m \sin(m\phi) \quad [5.2.13]$$

$$E_r^l(r > R) = \frac{ik_z^l}{\kappa_h}\sum_m (\alpha_m^+ H'^+_m + \alpha_m^- H'^-_m)\cos(m\phi) + \frac{i\omega}{r\kappa_h^2 c}\sum_m (\beta_m^+ H_m^+ + \beta_m^- H_m^-) m\cos(m\phi) \quad [5.2.14]$$

For the magnetic field

$$H_r^l(r \le R) = -\frac{i\epsilon_i\omega}{r\kappa_i^2 c}\sum_m a_m J_m m\sin(m\phi) + \frac{ik_z^l}{\kappa_{in}}\sum_m b_m J'_m \sin(m\phi) \quad [5.2.15]$$

$$H_r^l(r>R) = -\frac{i\epsilon_h\omega}{r\kappa_h^2 c}\sum_m(\alpha_m^+ H_m^+ + \alpha_m^- H_m^-)\, m\sin(m\phi) + \frac{ik_z^l}{\kappa_h}\sum_m(\beta_m^+ H'^+_m + \beta_m^- H'^-_m)\sin(m\phi) \quad [5.2.16]$$

The electric fields in the $\phi-$ direction

$$E_\phi^l(r\le R) = -\frac{ik_z^l}{\kappa_i^2 r}\sum_m a_m J_m m\sin(m\phi) - \frac{i\omega}{\kappa_i c}\sum_m b_m J'_m\sin(m\phi) \quad [5.2.17]$$

$$E_\phi^l(r>R) = -\frac{ik_z^l}{\kappa_h^2 r}\sum_m(\alpha_m^+ H_m^+ + \alpha_m^- H_m^-)\, m\sin(m\phi) - \frac{i\omega}{\kappa_h c}\sum_m(\beta_m^+ H'^+_m + \beta_m^- H'^-_m)\sin(m\phi) \quad [5.2.18]$$

The magnetic fields in the $\phi-$ direction

$$H_\phi^l(r\le R) = \frac{i\epsilon_i\omega}{\kappa_i c}\sum_m a_m J'_m\cos(m\phi) + \frac{ik_z^l}{r\kappa_i^2}\sum_m b_m J_m m\cos(m\phi) \quad [5.2.19]$$

$$H_\phi^l(r>R) = \frac{i\epsilon_h\omega}{\kappa_h c}\sum_m(\alpha_m^+ H'^+_m + \alpha_m^- H'^-_m)\cos(m\phi) + \frac{ik_z^l}{r\kappa_h^2}\sum_m(\beta_m^+ H_m^+ + \beta_m^- H_m^-)m\cos(m\phi) \quad [5.2.20]$$

5.3 Applying the boundary conditions at $r = R$

We begin by using the continuity of the tangential components of the electric and magnetic fields at $r = R$ to obtain an expression for $\{a_m, b_m\}$, $\{\alpha_m^+, \beta_m^+\}$ and $\{\alpha_m^-, \beta_m^-\}$. In the $z-$ direction

$$a_m J_m = \alpha_m^+ H_m^+ + \alpha_m^- H_m^- \quad [5.3.1]$$

$$b_m J_m = \beta_m^+ H_m^+ + \beta_m^- H_m^- \quad [5.3.2]$$

and in the $\phi-$ direction

$$\frac{k_z^l}{\kappa_i^2 R} a_m J_m m + \frac{\omega}{\kappa_i c} b_m J'_m = \frac{k_z^l}{\kappa_h^2 R} (\alpha_m^+ H_m^+ + \alpha_m^- H_m^-) m + \frac{\omega}{\kappa_h c} (\beta_m^+ H'^+_m + \beta_m^- H'^-_m) \quad [5.3.3]$$

$$\frac{\epsilon_i \omega}{\kappa_i c} a_m J'_m + \frac{k_z^l}{R\kappa_i^2} J_m m = \frac{\epsilon_h \omega}{\kappa_h c} (\alpha_m^+ H'^+_m + \alpha_m^- H'^-_m) + \frac{k_z^l}{R\kappa_h^2} (\beta_m^+ H_m^+ + \beta_m^- H_m^-) \quad [5.3.4]$$

After solving Eqs. (5.3.1) and(5.3.2) for $\{a_m, b_m\}$ and substituting these into Eqs.(5.3.3) and (5.3.4), we see that only one of the three sets of coefficients $\{a_m, b_m\}$,$\{\alpha_m^+, \beta_m^+\}$, and $\{\alpha_m^-, \beta_m^-\}$ is independent. Explicitly, the linear relationship

$$\begin{pmatrix} \alpha_m^+ \\ \vdots \\ \beta_m^+ \end{pmatrix} = \hat{S} \begin{pmatrix} \alpha_m^- \\ \vdots \\ \beta_m^- \end{pmatrix} \quad [5.3.5]$$

can be derived from

$$\begin{bmatrix} \frac{k_z^l m}{R}\left(\frac{1}{\kappa_i^2} - \frac{1}{\kappa_h^2}\right) H_m^+ & \frac{\omega}{c}\left(\frac{J'_m}{J_m}\frac{1}{\kappa_i} H_m^+ - \frac{1}{\kappa_h} H'^+_m\right) \\ \frac{\omega}{c}\left(\frac{\epsilon_i}{\kappa_i}\frac{J'_m}{J_m} H_m^+ - \frac{\epsilon_h}{\kappa_h} H'^+_m\right) & \frac{k_z^l m}{R}\left(\frac{1}{\kappa_i^2} - \frac{1}{\kappa_h^2}\right) H_m^+ \end{bmatrix} \begin{pmatrix} \alpha_m^+ \\ \beta_m^+ \end{pmatrix}$$

$$= \begin{bmatrix} \frac{k_z^l m}{R}\left(\frac{1}{\kappa_h^2} - \frac{1}{\kappa_i^2}\right) H_m^- & \frac{\omega}{c}\left(\frac{1}{\kappa_h} H'^-_m - \frac{J'_m}{J_m}\frac{1}{\kappa_i} H_m^-\right) \\ \frac{\omega}{c}\left(\frac{\epsilon_h}{\kappa_h} H'^-_m - \frac{\epsilon_i}{\kappa_i}\frac{J'_m}{J_m} H_m^-\right) & \frac{k_z^l m}{R}\left(\frac{1}{\kappa_h^2} - \frac{1}{\kappa_i^2}\right) H_m^- \end{bmatrix} \begin{pmatrix} \alpha_m^- \\ \beta_m^- \end{pmatrix} \quad [5.3.6]$$

where each of the four sub-matrices is a diagonal matrix with its elements corresponding to the Bessel function combinations evaluated at $r = R$. In this cylindrically-symmetric case, the S-matrix can be formally divided into four (diagonal) sub-matrices

$$\hat{S} = \begin{bmatrix} S_{11} & S_{12} \\ S_{21} & S_{22} \end{bmatrix} \quad [5.3.7]$$

The components S_{11} and S_{22} represent polarization-preserving TE-, TM-reflection, while the components S_{12}, S_{21} represent polarization-mixing coupling of TM to TE waves. Note that in the cylindrical geometry, polarization-preserving reflection is only possible when either $m = 0$ or $k_z = 0$, which yields $\det S_{12} = \det S_{21} = 0$.

Using Eqns. (5.3.1) and (5.3.2) allows one to calculate the amplitudes $\{a, b\}$ based on the amplitudes of $\{\alpha^-, \beta^-\}$. The field equations will provide complete information about the field distribution inside the unit cell once the parameters k_z^l, and $\{\alpha^-, \beta^-\}$ are known. In order to obtain the additional expressions needed to solve for these unknowns the periodicity of the unit cell must now be investigated.

5.4 Dispersion of the Longitudinal Mode

Let's now focus on the problem of calculating the dispersion of the mode. This reduces to the problem of calculating a relationship between internal structure of the unit cell and the set of parameters k_z^l, while $\{\alpha^-, \beta^-\}$ are known. For the square unit cell geometry, considered in this work, the latter combination will only contain cylindrical modes with m = 0,4,8,... The field of the eigenmode propagating in the periodic array of wires should satisfy the Bloch-periodicity condition

$$\left.\begin{matrix}E\\H\end{matrix}\right|_{x=-\frac{a}{2},y} = \left.\begin{matrix}E\\H\end{matrix}\right|_{x=+\frac{a}{2},y} \qquad [5.4.1]$$

Having this requirement we can write down the field equations using the projection $E_y, H_y = E_r, H_r \cos\phi + E_\phi, H_\phi \sin\phi$

$$E_y = \left[\frac{ik_z^l}{\kappa_h}\sum_m(\alpha_m^+ H'^+_m + \alpha_m^- H'^-_m)\cos(m\phi) + \frac{i\omega}{r\kappa_h^2 c}\sum_m(\beta_m^+ H_m^+ + \beta_m^- H_m^-)\, m\cos(m\phi)\right]\sin\phi - \left[\frac{ik_z}{\kappa_{out}^2 r}\sum_m(\alpha_m^+ H_m^+ + \alpha_m^- H_m^-)\, m\sin(m\phi) + \frac{i\omega}{\kappa_{out} c}\sum_m(\beta_m^+ H'^+_m + \beta_m^- H'^-_m)\sin(m\phi)\right]\cos\phi \qquad [5.4.2]$$

$$H_y = \left[-\frac{i\epsilon_h\omega}{r\kappa_h^2 c}\sum_m(\alpha_m^+ H_m^+ + \alpha_m^- H_m^-)\, m\sin(m\phi) + \frac{ik_z^l}{\kappa_{out}}\sum_m(\beta_m^+ H'^+_m + \beta_m^- H'^-_m)\sin(m\phi)\right]\sin\phi + \left[\frac{i\epsilon_h\omega}{\kappa_h c}\sum_m(\alpha_m^+ H'^+_m + \alpha_m^- H'^-_m)\cos(m\phi) + \frac{ik_z^l}{r\kappa_h^2}\sum_m(\beta_m^+ H_m^+ + \beta_m^- H_m^-)m\cos(m\phi)\right]\cos\phi \qquad [5.4.3]$$

Here we enforce periodicity of y −components of electric and magnetic fields. Although this condition should ideally be satisfied for all values of the y coordinate from the interval $y \in \left[-\frac{a}{2}, \frac{a}{2}\right]$, in practice it suffices to enforce the Bloch-periodicity condition for a number of fixed points $\{x_j, y_j\}$ equal to the number of m values in Eqs.(5.4.2) and (5.4.3). In the calculations we assume $y_j = \frac{a}{2\,N_m} j$, with N_m being the number of m terms. The analysis suggests that the choice of the exact location of the points does not significantly alter the dispersion of the mode, derived with the technique described below (see Fig 5.1).

Noting from symmetry that $\sin(\phi) = \sin(\pi - \phi)$, $\cos(\phi) = -\cos(\pi - \phi)$, $\sin(m\phi) = -\sin\big(m(\pi - \phi)\big)$, and $\cos(m\phi) = \cos\big(m(\pi - \phi)\big)$, it can be shown that components of electric and magnetic field possess the following identities:

$$E_y(x, y) = E_y(-x, y) \qquad [5.4.4]$$

$$H_y(x, y) = -H_y(-x, y) \qquad [5.4.5]$$

Therefore, Eq.(5.4.1) becomes equivalent to

$$\begin{pmatrix} \hat{0} & \hat{0} \\ \widehat{\widetilde{H}^{+}} & \widehat{H^{+}} \end{pmatrix}\begin{pmatrix} \alpha_m^{+} \\ \beta_m^{+} \end{pmatrix} + \begin{pmatrix} \hat{0} & \hat{0} \\ \widehat{\widetilde{H}^{-}} & \widehat{H^{-}} \end{pmatrix}\begin{pmatrix} \alpha_m^{-} \\ \beta_m^{-} \end{pmatrix} = \begin{pmatrix} 0 \\ 0 \end{pmatrix} \qquad [5.4.6]$$

where the elements of the sub-matrices $H^{\pm}$ are evaluated based on the longitudinal field equations according to the following rules: the sub-matrices $\widetilde{H}$ and H represent the TM- and TE-polarized magnetic field respectively; the superscript of the expression $[\pm]$ corresponds to the superscript of the Hankel function; and the jm-th element of the sub-matrix represent the y-component of the magnetic field due to m-th Hankel function, evaluated at the point $\{x_j, y_j\} = \left\{\frac{a}{2}, y_j\right\}$. With the help of the S matrix, Eq.(5.4.6) can be further simplified as

$$\begin{pmatrix} \hat{0} & \hat{0} \\ \widehat{\widetilde{H}^{+}}\widehat{S_{11}} + \widehat{H^{+}}\widehat{S_{21}} + \widehat{\widetilde{H}^{-}} & \widehat{\widetilde{H}^{+}}\widehat{S_{12}} + \widehat{H^{+}}\widehat{S_{22}} + \widehat{H^{-}} \end{pmatrix}\begin{pmatrix} \alpha_m^{-} \\ \beta_m^{-} \end{pmatrix} = \begin{pmatrix} 0 \\ 0 \end{pmatrix} \qquad [5.4.7]$$

Finally, the amplitudes of the field of longitudinal TM-polarized wave are represented as $\begin{pmatrix} \alpha_m^{-} \\ 0 \end{pmatrix}$ with values of the coefficients α given by non-trivial solutions of the linear relationship

$$\left(\widehat{\mathcal{H}_y}\right)\alpha^- = \left(\widehat{\widehat{H}^+}\widehat{S_{11}} + \widehat{H^+}\widehat{S_{21}} + \widehat{\widehat{H}^-}\right)\alpha^- = 0 \qquad [5.4.8]$$

It is now easy to see that the dispersion of this wave is given by

$$\det\left|\widehat{\mathcal{H}_y}\right| = 0 \qquad [5.4.9]$$

To verify the validity of Eq.(5.4.9), the dispersion of the longitudinal wave corresponding to (i) $m = 0{,}4$ and (ii) $m = 0{,}4{,}8$ is calculated and compared with the derived dispersions to numerical solutions of Maxwell's equations. To summarize the results of these calculations in Fig. 5.1. It is clearly seen that even the rough approximation with $m = 0{,}4$ yields relatively good agreement with numerical solutions of Maxwell's equations. Including one extra harmonic makes agreement almost perfect. For the rest of this work we use the results corresponding to $m = 0, 4, 8$.

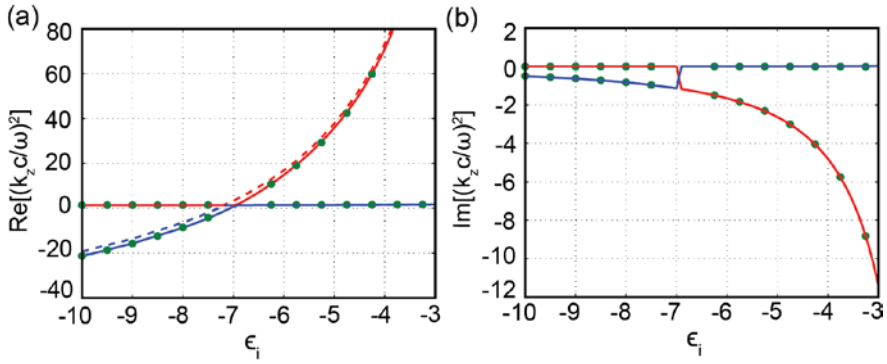

Figure 5.1: Propagation constant of the TM-polarized waves in nanowire composite as a function of wire permittivity. Lines and dashes represent Eqn. (5.4.9) for *m*=0,4,8 and *m*=0,4 respectively; symbols represent the numerical solutions to Maxwell's equations.

Now that the longitudinal dispersion is realized the remaining coefficients can be solved and an analytical result of the wave profiles can be produced. These results are in excellent agreement with the numerical calculations previously obtained. The fields generated using the longitudinal

field equations in comparison with the FEM field profiles show striking similarities (Fig. 5.2) and (Fig. 5.3).

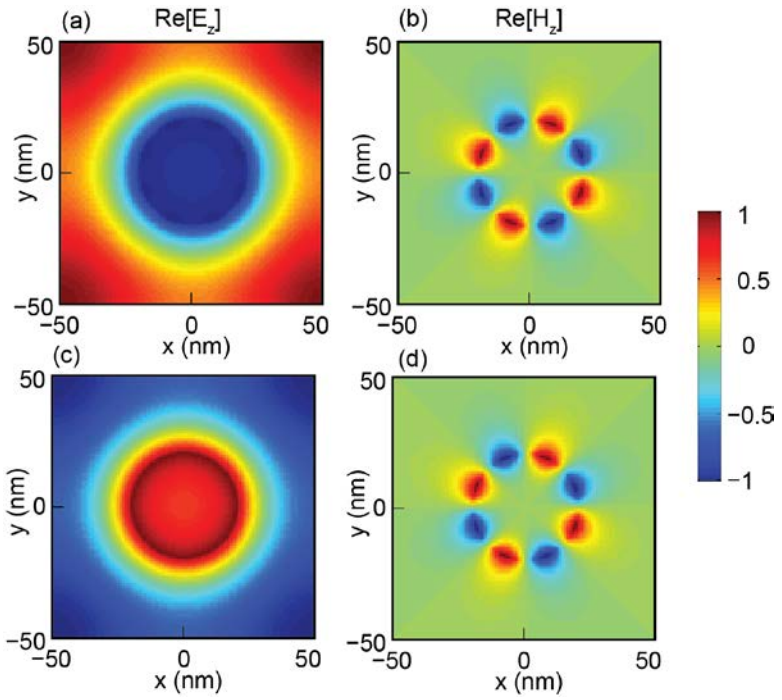

Figure 5.2: Analytical electric and magnetic fields within the unit cell produced using the previously derived field expressions, (a,b) corresponds to $\epsilon_i = -4 - 0.1i$ and (c,d) to $\epsilon_i = -9 - 0.1i$.

Notice that Since $\langle E_z \rangle \neq 0$, this verifies that the solution represents the longitudinal wave with dispersion $\epsilon_z(k_z) = 0$.

Fig. 5.3 demonstrates the excellent agreement between the numerical and analytical solutions corresponding to a three-term series $m = 0, 4, 8$, and clearly demonstrates the longitudinal character of this mode. This wave is strongly dispersive in the regime $\epsilon_i \to \epsilon_h$, corresponding to the surface plasmon oscillations on the metal-dielectric interface. On the other hand, when $-\epsilon_i \gg \epsilon_h$ (realized at mid-IR and lower frequencies for noble metals), the wavevector of the longitudinal mode approaches $n_\infty^l \omega/c$, and its transverse counterpart approaches the light line(see [24] and Fig.2).

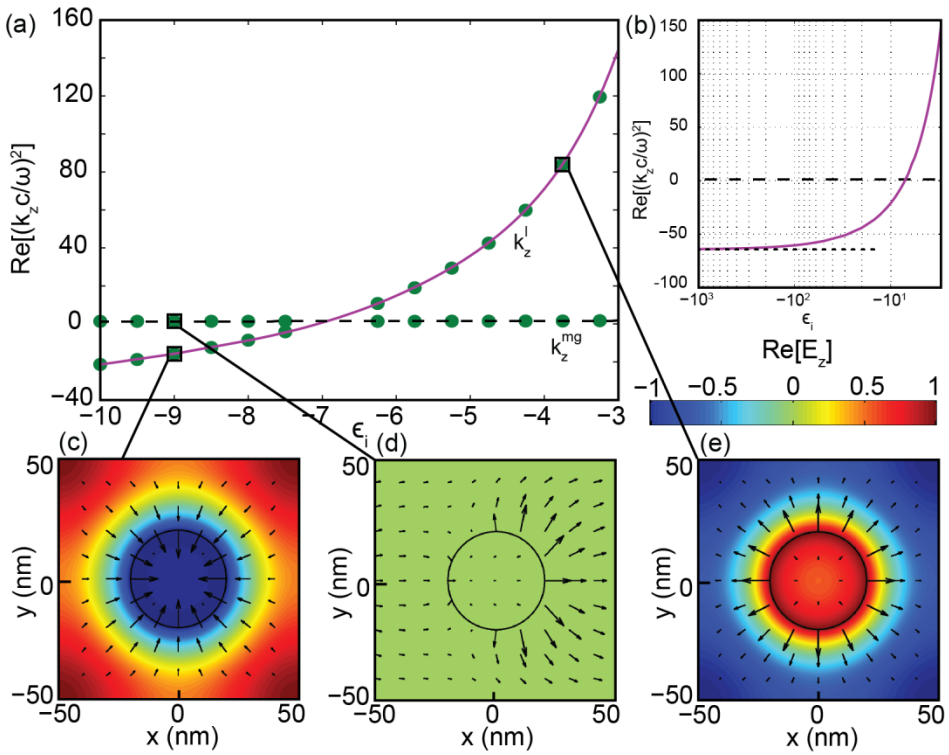

Figure 5.3: (a,b) Dispersion in nanowire composite as a function of wire permittivity. Dashed and solid lines represent transverse and longitudinal waves k_z^{mg} and k_z^l, eqn. (5.4.9) respectively, symbols represent numerical solutions to Maxwell's equations; for $-\epsilon_i \gg \epsilon_i, k_z^l \to n_\infty^l \omega/c$ (dotted line in (b)). (c,d,e) electric field in the unit cell; surface plots and arrows represent E_z and $\vec{E}_{x,y}$ components, respectively.

6 Solutions at Oblique Angles

The next step is to obtain the dispersion and field profiles for angles other than incident. To achieve this we use the previous derived results for the longitudinal wave, which describes the microscopic field, and those obtained from effective medium theory (EMT), the macroscopic field. Coupling these modes together through the use of the coupled oscillator model a complete description of the nonlocal effective permittivity can be obtained.

$$\epsilon_z(k_z) = \xi\left(k_z^2 - {k_z^l}^2\right)\frac{c^2}{\omega^2} \qquad [6.1]$$

where k_z is the wavevector of the mode in the nolocal effective medium approximation, k_z^l is the wavevector of the mode composite in the microscopic theory, and ξ is the factor which will be determined below.

Eqn. (6.1) can be used along with the above considerations to determine the complete nonlocal dispersion for propagation at an angle to the optical axis. For simplicity, we consider the case $k_y = 0$, $k_x \neq 0$. Using egns. (2.2.14) and (2.2.15) where the propagation of the TM-polarized wave can be described by $\epsilon_z(k_z)\left(k_z^2 - \epsilon_{x,y}^{mg}\frac{\omega^2}{c^2}\right) = -\epsilon_{x,y}^{mg}k_x^2$. By substituting Eq.(6.1) in this equation, we obtain the following relation

$$\left(k_z^2 - {k_z^l}^2\right)\left(k_z^2 - \epsilon_{x,y}^{mg}\frac{\omega^2}{c^2}\right) = -\frac{\epsilon_{x,y}^{mg}}{\xi}\frac{\omega^2}{c^2}k_x^2. \qquad [6.2]$$

Similar to other nonlocal materials, nanowire materials support two TM-polarized waves propagating with different indices

$$k_z = \sqrt{\frac{\left(k_z^{l\,2} + \epsilon_{x,y}^{mg}\frac{\omega^2}{c^2}\right) \pm \sqrt{\left(k_z^{l\,2} + \epsilon_{x,y}^{mg}\frac{\omega^2}{c^2}\right)^2 - 4\frac{\epsilon_{x,y}^{mg}}{\xi}\left(\frac{\omega^2}{c^2}\right)^2 k_x^2}}{2}} \qquad [6.3]$$

The final free parameter of the model, multiplicative factor ξ, can be determined by requiring that in the limit of small k_x the properties of one of the two TM-modes follow elliptical or hyperbolic dispersion and has $k_z(k_x) = const$ dependence that is observed in the wire media when $\epsilon_z^{mg} > 0$, $\epsilon_z^{mg} \lesssim 0$, and $\epsilon_z^{mg} \ll -1$ respectively [6,24,30,39,42,43]. The relationship

$$\xi = p\frac{\epsilon_i + \epsilon_h}{\epsilon_h - n_l^{\infty\,2}} \qquad [6.4]$$

adequately describes optics of wire media in these three limits. The excellent agreement between the predictions of Eq. (6.3) and the full-wave numerical solutions of Maxwell's equations are shown in Fig. 6.1.

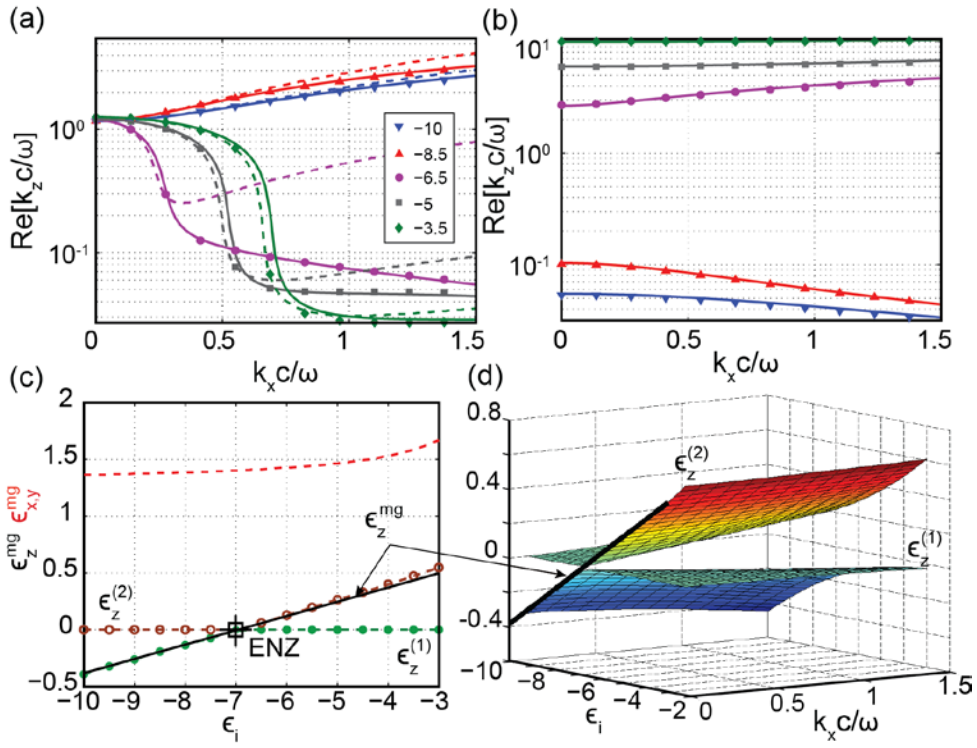

Figure 6.1: (a,b) Isofrequency contours of TM-polarized modes in nanowire composites. Solid lines and symbols correspond to Eq.(6.3) and numerical solutions of Maxwell equations respectively; dashed lines represent local EMT. (c,d) The effecttive medium permittivity of nonlocal nanowire composite for $k_x = 0$ (c) and for $k_x \neq 0$ (d); $\epsilon_z^{(1)}$, $\epsilon_z^{(2)}$ represent two solutions of Eq.(6.1); cross marks ENZ condition ($\epsilon_z^{mg} \cong 0$).

As expected the isofrequency of the "main" TM-polarized wave resembles and ellipse or hyperbola which for small values of k_x is well described by $\hat{\epsilon}^{mg}$. At the same time, the dependence $k_z(k_x)$ for the "additional" TM-wave is opposite to that of its "main" counterpart. The z-component of the permittivity can be described by Eq. (2.1.11) when $k_x = 0$, but for oblique angles exhibits strong spatial dispersion.

To further validate our analytical approach we analyzed the optical properties of the system with permittivity of the host material $\epsilon_h = 2.25$. Such a comparison is shown in Fig. 5.4. It is clearly seen that the developed technique is in excellent agreement with numerical solutions of Maxwell equations. In contrast, local EMT adequately predicts response of the nanowire system only outside ENZ region, and only for almost-normal propagation $k_x \ll \omega/c$.

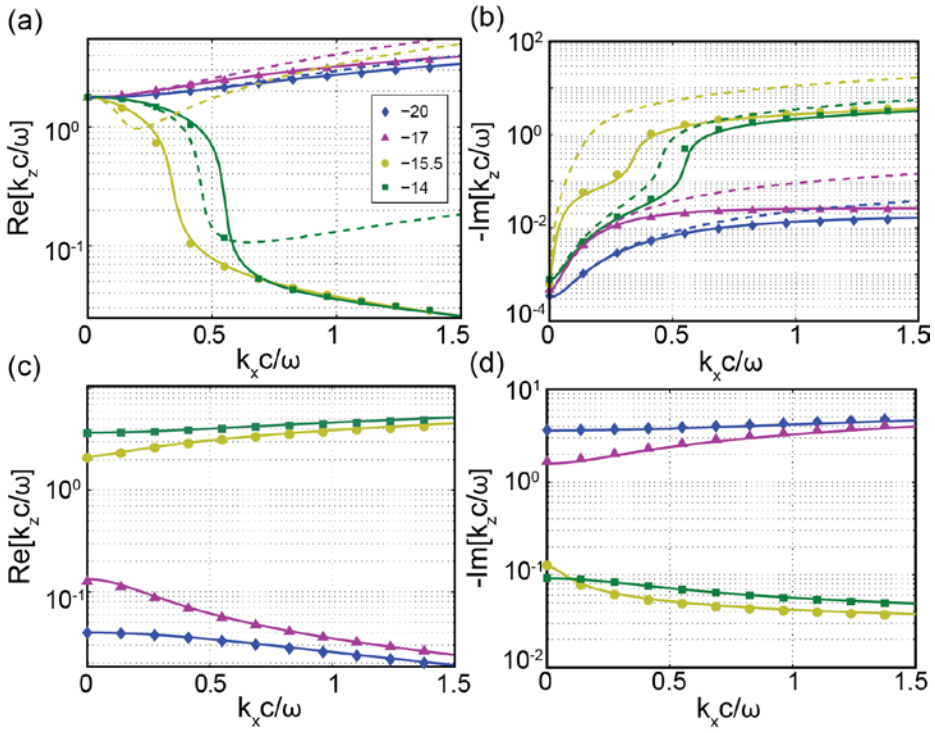

Figure 6.2: (a,b) Isofrequency contours of TM-polarized modes in nanowire composites for the composite with $\epsilon_h = 2.25$; (c,d) Isofrequency contours for additional TM-polarized mode for the same system

6.1 Wave profiles at oblique angles

Now that the origin and dispersion of the modes propagating in nanowire systems is understood, let's focus on the analysis of the optical properties of finite-size wire arrays. Since in the EMT approximation the fields of TE and TM-polarized modes are orthogonal to each other, and since propagation of TE polarized light through the wire-based system is only affected by x, y-components of the permittivity, this propagation can be successfully described by Eqs.(2.1.11) and (2.1.12).

Here, we focus on the analysis of propagation of TM-polarized light. This analysis must describe the structure of electromagnetic waves propagating in the system, and determine what additional

boundary conditions needed to calculate the amplitudes of the two TM-polarized modes inside the wire system.

Consistency with the effective medium description requires that the unit-cell averaged fields satisfy both constituent relations $\epsilon_j = \langle \epsilon E_j \rangle / \langle E_j \rangle$ and relations between the field components of the plane wave $\langle \epsilon E_z \rangle = -k_x/k_z \langle \epsilon E_x \rangle$. With these constraints, we start with Eqs.(2.1.11) and (2.1.12) and the field solutions derived in Ch.5. One can determine the parameters α_0^-, $\mathfrak{e}_z^{mg}$, and $\mathfrak{e}_x^{mg}$ by normalizing $\langle E_z^l \rangle = \langle E_x^{mg} \rangle = \langle E_z^{mg} \rangle = 1$, and constructing the fields of the two waves propagating in the wire media as $\vec{E}(x,y)e^{i\omega t - ik_x x - ik_z z}$ with

$$E_x(x,y) = E_x^{mg} \tag{6.1.1}$$

$$E_z(x,y) = \gamma^{mg} E_z^{mg} + \gamma^l E_z^l|_{z=0} \tag{6.1.2}$$

Using the above expressions we arrive at

$$\gamma^{mg} = -\frac{\epsilon_{x,y}^{mg} k_x}{\epsilon_z k_z} \frac{\epsilon_z - \epsilon^l}{\epsilon_z^{mg} - \epsilon^l} \tag{6.1.3}$$

$$\gamma^l = -\frac{\epsilon_{x,y}^{mg} k_x}{\epsilon_z k_z} \frac{\epsilon_z - \epsilon_z^e}{\epsilon^l - \epsilon_z^e} \tag{6.1.4}$$

In Eqs.(6.1.3) and (6.1.4) $\epsilon_z \equiv \epsilon(k_z)$ which is given by eqn. (6.1) $k_z(k_x)$ by eqn. (6.3), and $\epsilon^l = \langle \epsilon(x,y) E_z^l(x,y) \rangle / \langle E_z^l(x,y) \rangle$.

Eq.(6.1.2) represents a transition between full-wave solutions of Maxwell's equations in the nanowire array where the fields oscillate on the scale of the individual wires, and effective-medium solutions where plane waves propagate in the homogenized material. Since our model for $\vec{E}^{mg}$ assumes quasistatic limit, Eq.(6.1.2) is technically valid in the limit $a \ll 2\pi/k_x$, λ_0. However, Fig. 6.1 indicates that the developed formalism also provides adequate approximation for optics of wire systems for higher values of k_x.

7 Transmission and Reflection

We now consider the problem of reflection/refraction of light at the interface of two (nonlocal) (meta-) materials, extending the well-developed transfer-matrix formalism [56,57] to nonlocal composites.

7.1 Transfer Matrix formalism

The typical geometry of light propagation through a finite-thickness slab of nanowire material is shown in Fig.7.1. For this geometry, Maxwell's equations require continuity of (microscopic) E_x and D_z fields. Conventional effective-medium boundary conditions are obtained by averaging these relationships across the unit cell [6,28,30,39,40]. However, nanowire media support two TM-polarized modes resulting in four TM-polarized waves propagating in the finite-thickness slab (see Fig.7.1). Therefore, calculation of the amplitudes of these waves requires additional boundary conditions (ABCs). Different forms of ABCs, often based on heuristic arguments have been suggested in previous works [16,22]. Here we present a first-principles approach to solve this long-standing problem.

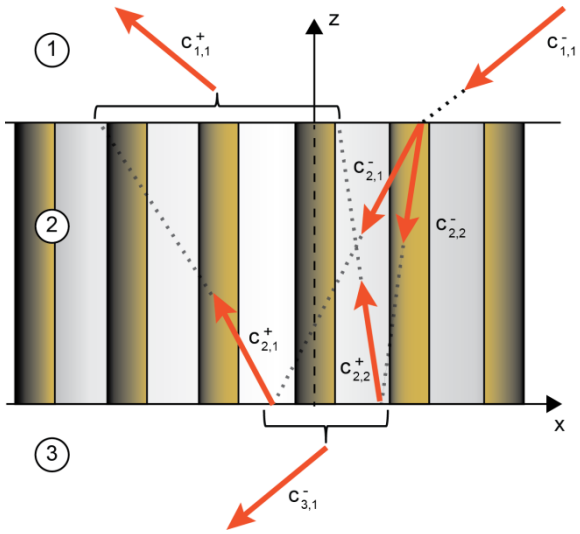

Figure 7.1: Schematic of TMM for a nanowire composite. Each mode is labeled to clarify notation as well as interface numbers.

Maxwell's equations require continuity of (microscopic) E_x and D_z and the effective-medium boundary conditions and is obtained by averaging these relationships across the unit cell. Multiple, linearly independent boundary conditions can be obtained by requiring the continuity of $\mathbb{E}^n = \langle e^{2\pi i n \frac{x}{a}} E_x \rangle$ and $\mathbb{D}^n = \langle e^{2\pi i n \frac{x}{a}} D_z \rangle$ with different integer n.

Continuity of $\mathbb{E}^0$ and $\mathbb{D}^0$ yields conventional EMT; continuity of $\mathbb{D}^1$ [and, in case of contact of two nonlocal media, of $\mathbb{E}^1$] represents the set of ABCs. For example, assuming that the top interface is located at $z = z_0$, the boundary conditions for this interface are implemented as:

$$\begin{cases} c_{1,1}^{+}\mathbb{E}_{1,1}^{0} e^{ik_{z_{1,1}} z_0} + c_{1,1}^{-}\mathbb{E}_{1,1}^{0} e^{-ik_{z_{1,1}} z_0} = \sum_{l=1,2} c_{2,l}^{+}\mathbb{E}_{2,l}^{0} e^{ik_{z_{2,l}} z_0} + c_{2,l}^{-}\mathbb{E}_{2,l}^{0} e^{-ik_{z_{2,l}} z_0} \\ c_{1,1}^{+}\mathbb{D}_{1,1}^{0} e^{ik_{z_{1,1}} z_0} - c_{1,1}^{-}\mathbb{D}_{1,1}^{0} e^{-ik_{z_{1,1}} z_0} = \sum_{l=1,2} c_{2,l}^{+}\mathbb{D}_{2,l}^{0} e^{ik_{z_{2,l}} z_0} - c_{2,l}^{-}\mathbb{D}_{2,l}^{0} e^{-ik_{z_{2,l}} z_0} \\ c_{1,1}^{+}\mathbb{D}_{1,1}^{1} e^{ik_{z_{1,1}} z_0} - c_{1,1}^{-}\mathbb{D}_{1,1}^{1} e^{-ik_{z_{1,1}} z_0} = \sum_{l=1,2} c_{2,l}^{+}\mathbb{D}_{2,l}^{1} e^{ik_{z_{2,l}} z_0} - c_{2,l}^{-}\mathbb{D}_{2,l}^{1} e^{-ik_{z_{2,l}} z_0} \end{cases} \quad [7.1.1]$$

In the expressions above the double-subscript represents the layer number in the system and the mode number within the layer, while the "$\pm$" superscript represent the direction of the wave propagation (see Fig. 7.1). The amplitudes of the wave propagating in the system represent the amplitude of $\mathbb{E}^0$; therefore, the amplitudes of E_x are symmetric with respect to change of propagation direction $k_z \to -k_z$, while the amplitudes of E_z, D_z are anti-symmetric

Eq.(7.1.1) can be straightforwardly used as a building block to implement the nonlocal analog of transfer-matrix formalism, calculating transmission, reflection, and field distributions across an arbitrary planar stack containing nanowire composites.

As before, two sets of numerical calculations were used, commercial finite-element solver and in-house RCWA code. Since both sets of calculations utilized full 3D geometry of the unit cell of finite-length wire array, and since solutions of Maxwell's equations in 3D geometry

are known to be challenging, we analyzed the stability of results of our calculations. To assess the accuracy of RCWA calculations, the number of Fourier harmonics in representation of spatial profile of permittivity was varied. Similarly, the mesh size in finite-element calculations is varied and the stability of the solutions with respect to minor modification of the geometry are checked. In particular, the cap parts of the wires were changed from the planar to ellipsoidal shape [see Fig.7.2]. The results of these studies are summarized in Fig.7.2. Note that according to finite-element calculations, transmission and reflection profiles strongly depend on the geometry for $\epsilon_i \simeq -3$. Analysis of the field profiles in this spectral range suggests that these minima are artifacts of meshing routines implemented in the FEM solver. To mitigate these artifacts, we show the average of these results.

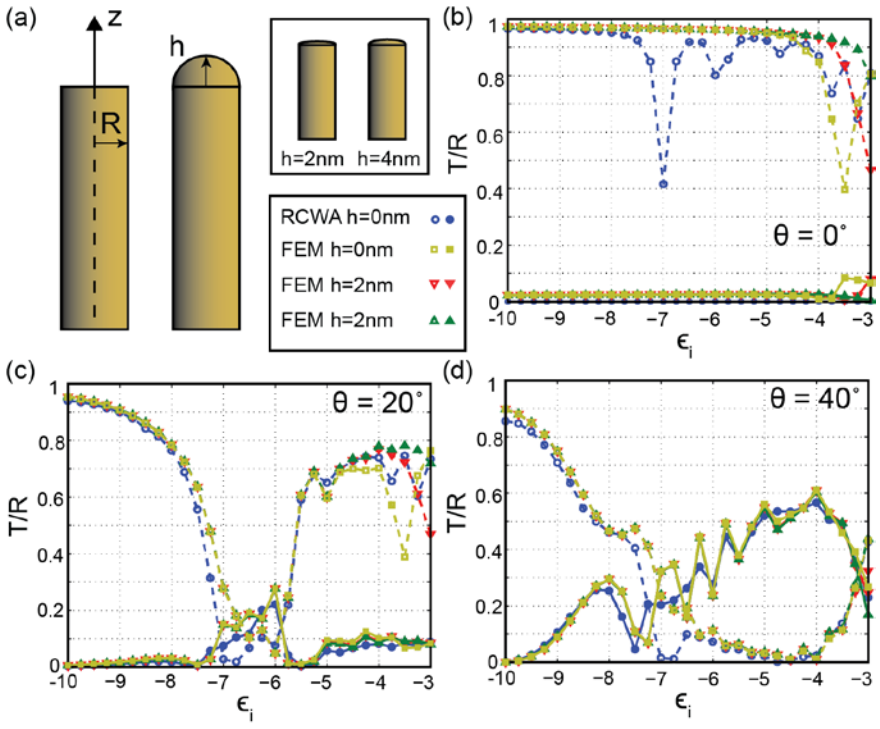

Figure 7.2: (a) Schematic of different nanowire geometry used in finite-element numerical solutions of Maxwell equations; inset shows to-scale geometry; (b-d) Transmission and reflection of light through a parallel slab of nanowire media, suspended in air with nanowires with $Im(\epsilon_i) = -0.1$ at various angles for different nanowire geometry and solution method.

Transmission and reflection of the nanowire metamaterial are now compared for full-vectorial numerical solutions of Maxwell's equations predictions of conventional (local) effective medium theory, and predictions of the nonlocal EMT developed in this work in Fig.7.3. It is seen the smaller the loss and the larger the angle of incidence the more important it becomes to take into account the nonlocal optics of nanowire composites. Interestingly, nonlocal response strongly affects optical response of the wire metamaterials across the broad range of the effective permittivities. This effect most clearly seen in reflection, but is also visible in transmission, especially in ENZ regime.

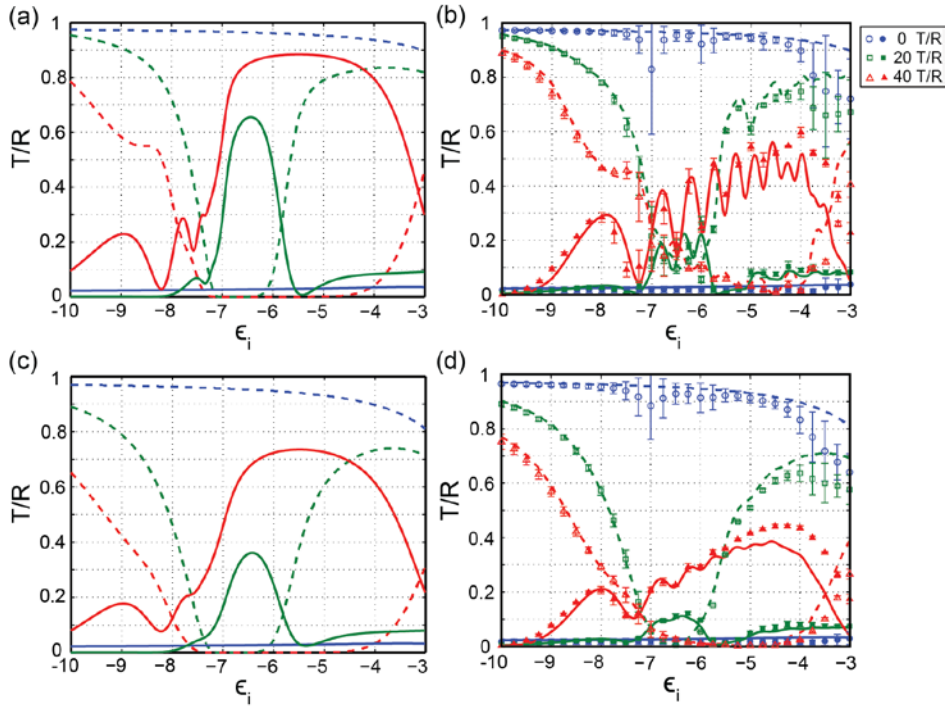

Figure 7.3: Transmission and reflection of light through a parallel slab of nanowire media, suspended in air with $Im(\epsilon_i) = -0.1$ (a,b) and $Im(\epsilon_i) = -0.25$ (c,d). (a,c): local TMM calculations, (b,d): nonlocal EMT developed here (lines) and numerical solutions of Maxwell equations (symbols); Solid lines and filled symbols represent reflection, dashed lines and empty symbols - transmission.

To further validate the developed approach, we calculated transmission and reflection for a planar slab of nanowire material with permittivity of the host $\epsilon_h = 2.25$. A comparison

between the numerical solutions of Maxwell's equations, predictions of local EMT, and nonlocal EMT is shown in Fig.7.4. We again note that the nonlocal EMT provides a substantially more accurate description of optics of nanowire systems than its local counterpart.

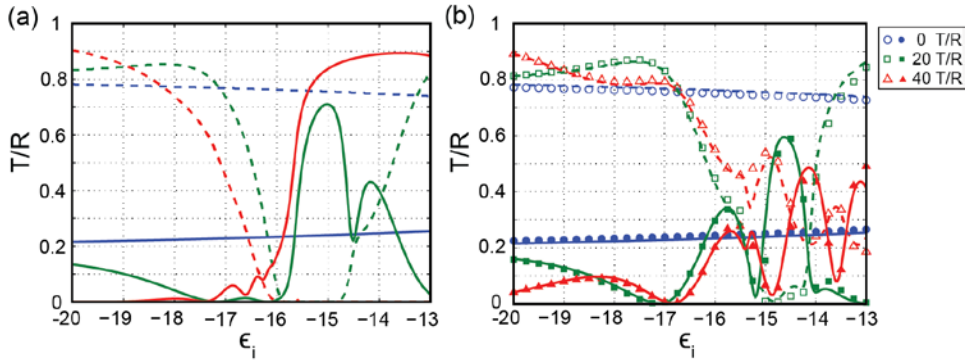

Figure 7.4: Transmission and reflection of light through a parallel slab of nanowire material suspended in a substrate with $\epsilon_h = 2.25$ and $Im(\epsilon_i) = -0.1$. (a) Local calculations and (b) nonlocal EMT (lines) and numerical solutions to Maxwell's equations (symbols).

To assess the robustness of the developed formalism, we compared transmission and reflection of light by nanowire arrays calculated with the developed nonlocal EMT and with numerical solutions of Maxwell's equations.

8 Conclusion

To conclude, an approach to describe the optics governing nonlocal wire metamaterials across the whole optical spectrum was presented. This formalism demonstrates excellent agreement with the results of numerical solutions to Maxwell's equations and is essential in the development of an adequate description of optics in wire arrays. This facilitates understanding the true density of photonic states through the limits of resolution in these systems.

The formalism can be expanded to calculate the field inside the structures with more complicated unit cells, that include multi-shelled wires, coax-cable-like systems, etc. [52,53] and can be further extended to calculate fields inside the systems with a non-circular cross-section of wires, in which case the S-matix ceases to be block-diagonal [54,55]. A mechanism is also provided to explain the deviation for the dispersion of the waves in nanowire materials from the prediction of local effective medium technique. In particular, this deviation places fundamental limits on subwavelengh light manipulation, and on the increase of the local density of photonics states [21].

9 Future Work

The developed analytical model that adequately describes the steady-state single-frequency response for nanowire systems can be straightforwardly be adapted to wire structures with non-square unit cells as well as to wire-like composites, e.g multi-shelled wires, and coax-cable-like systems. The formalism can also be used as a platform for analysis of complex light interaction with anisotropic plasmonic composites.

Our next major task is to form an understanding of the light emission in nanowire metamaterials. It is well known that light emission by dyes, quantum dots, and other quantum mechanical systems can be substantially altered by the surrounding materials. Due to the correlation between light emission and the density of states, any modulation of the local density of states is known to lead to enhancement (or quenching) of fluorescence rates of emitters in proximity to metal nanostructures [58-61].

Emission properties are further modified in hyperbolic systems that in effective medium approximation possess singular density of states over a significant frequency range [62,63]. However, while it is clear that nonlocality will significantly affect emission in metamaterials with large (or small) values of effective parameters, the very definition of density of optical states in nonlocal systems is not completely understood. Future work is to develop an understanding of interaction between nonlocal metamaterials and light-emitting systems.

References

[1] Engheta, Nader. "Circuits with light at nanoscales: optical nanocircuits inspired by metamaterials." *Science* 317.5845 (2007): 1698-1702.

[2] Pendry, John B., and David R. Smith. "Reversing light with negative refraction." *Physics Today* 57 (2004): 37-43.

[3] Shalaev, Vladimir M. "Optical negative-index metamaterials." *Nature photonics* 1.1 (2007): 41-48.

[4] Pendry, John B., D. Schurig, and David R. Smith. "Controlling electromagnetic fields." *Science* 312.5781 (2006): 1780-1782.

[5] Cai, Wenshan, et al. "Optical cloaking with metamaterials." *Nature photonics* 1.4 (2007): 224-227.

[6] Atkinson, Ron, et al. "Anisotropic optical properties of arrays of gold nanorods embedded in alumina." *Physical Review B* 73.23 (2006): 235402.

[7] Yao, Jie, et al. "Optical negative refraction in bulk metamaterials of nanowires." *Science* 321.5891 (2008): 930-930.

[8] Casse, B. D. F., et al. "Super-resolution imaging using a three-dimensional metamaterials nanolens." *Applied Physics Letters* 96.2 (2010): 023114-023114.

[9] Silveirinha, Mário, and Nader Engheta. "Tunneling of electromagnetic energy through subwavelength channels and bends using ε-near-zero materials." *Physical review letters* 97.15 (2006): 157403.

[10] Belov, Pavel A., et al. "Transmission of images with subwavelength resolution to distances of several wavelengths in the microwave range." *Physical Review B* 77.19 (2008): 193108.

[11] Thongrattanasiri, Sukosin, and Viktor A. Podolskiy. "Hypergratings: nanophotonics in planar anisotropic metamaterials." *Optics letters* 34.7 (2009): 890-892.

[12] Liu, Zhaowei, et al. "Far-field optical hyperlens magnifying sub-diffraction-limited objects." *science* 315.5819 (2007): 1686-1686.

[13] Salandrino, Alessandro, and Nader Engheta. "Far-field subdiffraction optical microscopy using metamaterial crystals: Theory and simulations." *Physical Review B* 74.7 (2006): 075103.

[14] Liu, Zhaowei, et al. "Far-field optical hyperlens magnifying sub-diffraction-limited objects." *science* 315.5819 (2007): 1686-1686.

[15] Cai, Wenshan, et al. "Optical cloaking with metamaterials." *Nature photonics* 1.4 (2007): 224-227.

[16] Pollard, R. J., et al. "Optical nonlocalities and additional waves in epsilon-near-zero metamaterials." *Physical review letters* 102.12 (2009): 127405.

[17] Simovski, Constantin R., et al. "Wire metamaterials: Physics and applications." *Advanced Materials* 24.31 (2012): 4229-4248.

[18] Tumkur, T. U., et al. "Control of absorption with hyperbolic metamaterials." *Applied Physics Letters* 100.16 (2012): 161103-161103.

[19] Poddubny, Alexander N., Pavel A. Belov, and Yuri S. Kivshar. "Spontaneous radiation of a finite-size dipole emitter in hyperbolic media." *Physical Review A* 84.2 (2011): 023807.

[20] Kidwai, Omar, Sergei V. Zhukovsky, and J. E. Sipe. "Effective-medium approach to planar multilayer hyperbolic metamaterials: Strengths and limitations." *Physical Review A* 85.5 (2012): 053842.

[21] Yan, Wei, Martijn Wubs, and N. Asger Mortensen. "Hyperbolic metamaterials: Nonlocal response regularizes broadband supersingularity." *Physical Review B* 86.20 (2012): 205429.

[22] Pekar, S. I. "Zh Eksper. Teor. Fiz. 33, 1022 (1957)[Sov. Phys. JETP 6, 785 (1958)]; ibid. Fiz. Tvers. Tela Leningrad 4, 1031 (1962)." *Sov. Phys. Solid State* 4 (1962): 953.

[23] Agranovich, Vladimir Moiseevich, and Vitaliĭ Lazarevich Ginzburg. *Crystal optics with spatial dispersion, and excitons*. Berlin-Heidelberg: Springer-Verlag, 1984.

[24] Silveirinha, Mário G. "Nonlocal homogenization model for a periodic array of ϵ-negative rods." *Physical Review E* 73.4 (2006): 046612.

[26] Burgos, Stanley P., et al. "A single-layer wide-angle negative-index metamaterial at visible frequencies." *Nature Materials* 9.5 (2010): 407-412.

[27] Noginov, Mikhail, et al. "Focus issue: hyperbolic metamaterials." *Optics express* 21.12 (2013): 14895-14897.

[28] J.C.M. Garnett, Philos. Trans. R. Soc. London, Ser. B 203, 385 (1904).

[30] Elser, Justin, et al. "Nanowire metamaterials with extreme optical anisotropy." *Applied physics letters* 89.26 (2006): 261102-261102.

[31] Ziolkowski, Richard W. "Propagation in and scattering from a matched metamaterial having a zero index of refraction." *Physical Review E* 70.4 (2004): 046608.

[32] Silveirinha, Mário, and Nader Engheta. "Tunneling of electromagnetic energy through subwavelength channels and bends using ε-near-zero materials." *Physical review letters* 97.15 (2006): 157403.

[33] Engheta, Nader. "Pursuing Near-Zero Response." *Science* 340.6130 (2013): 286-287.

[34] Cortes, C. L., et al. "Quantum nanophotonics using hyperbolic metamaterials." *Journal of Optics* 14.6 (2012): 063001.

[35] Ginzburg, V. L. "Electromagnetic waves in isotropic and crystalline media characterized by dielectric permittivity with spatial dispersion." *JETP* 34 (1958): 1096.

[36] Kabashin, A. V., et al. "Plasmonic nanorod metamaterials for biosensing." *Nature materials* 8.11 (2009): 867-871.

[37] COMSOL Multiphysics, www.comsol.com

[38] Moharam, M. G., and T. K. Gaylord. "Rigorous coupled-wave analysis of planar-grating diffraction." *JOSA* 71.7 (1981): 811-818.

[39] Sarychev, Andrey K., R. C. McPhedran, and Vladimir M. Shalaev. "Electrodynamics of metal-dielectric composites and electromagnetic crystals." *Physical Review B* 62.12 (2000): 8531.

[40] Wurtz, G. A., et al. "Guided plasmonic modes in nanorod assemblies: strong electromagnetic coupling regime." *Optics express* 16.10 (2008): 7460-7470.

[41] Pokrovsky, A. L., and A. L. Efros. "Nonlocal electrodynamics of two-dimensional wire mesh photonic crystals." *Physical Review B* 65.4 (2002): 045110.

[42] Belov, P. A., et al. "Strong spatial dispersion in wire media in the very large wavelength limit." *Physical Review B* 67.11 (2003): 113103.

[43] Silveirinha, Mário G., Pavel A. Belov, and Constantin R. Simovski. "Subwavelength imaging at infrared frequencies using an array of metallic nanorods." *Physical Review B* 75.3 (2007): 035108.

[44] Hopfield, J. J., and D. G. Thomas. "Theoretical and experimental effects of spatial dispersion on the optical properties of crystals." *Physical Review* 132.2 (1963): 563.

[45] Coleman, Thomas F., and Yuying Li. "An interior trust region approach for nonlinear minimization subject to bounds." *SIAM Journal on optimization* 6.2 (1996): 418-445.

[46] Coleman, Thomas F., and Yuying Li. "A reflective Newton method for minimizing a quadratic function subject to bounds on some of the variables." *SIAM Journal on Optimization* 6.4 (1996): 1040-1058.

[47] Dennis Jr, John E., David M. Gay, and Roy E. Walsh. "An adaptive nonlinear least-squares algorithm." *ACM Transactions on Mathematical Software (TOMS)* 7.3 (1981): 348-368.

[48] Levenberg, Kenneth. "A method for the solution of certain problems in least squares." *Quarterly of applied mathematics* 2 (1944): 164-168.

[49] Marquardt, Donald W. "An algorithm for least-squares estimation of nonlinear parameters." *Journal of the Society for Industrial & Applied Mathematics* 11.2 (1963): 431-441.

[50] Boggs, Paul T., Richard H. Byrd, and Robert B. Schnabel. "A stable and efficient algorithm for nonlinear orthogonal distance regression." *SIAM Journal on Scientific and Statistical Computing* 8.6 (1987): 1052-1078.

[51] Landau, L. D., E. M. Lifshitz, and L. P. Pitaevskii. "Electrodynamics of continuous media, vol. 8." *Course of theoretical physics* (1984): 45-47.

[52] Burgos, Stanley P., et al. "A single-layer wide-angle negative-index metamaterial at visible frequencies." *Nature Materials* 9.5 (2010): 407-412.

[53] Prokes, S. M., et al. "Hyperbolic and plasmonic properties of Silicon/Ag aligned nanowire arrays." *Optics Express* 21.12 (2013): 14962-14974.

[54] Doron, Eyal, and Uzy Smilansky. "Chaotic spectroscopy." *Physical review letters* 68.9 (1992): 1255.

[55] Podolskiy, Viktor A., et al. "Chaotic microlasers based on dynamical localization." *Proceedings of the National Academy of Sciences of the United States of America* 101.29 (2004): 10498-10500.

[56] Rytov, S. M. "Electromagnetic properties of a finely stratified medium." *Sov. Phys. JETP* 2.3 (1956): 466-475.

[57] Yeh, Pochi, Amnon Yariv, and Chi-Shain Hong. "Electromagnetic propagation in periodic stratified media. I. General theory." *Journal of the Optical Society of America* 67.4 (1977): 423-438.

[58] E.M. Purcell, *"Spontaneous Emissin Probabilities at Radio Frequencies"* Phys. Rev. 11-12, p.681 (1946)

[59] J. R Lakowicz, J. Malicka, I. Gryczynski, Z. Gryczynski, and C. D Geddes, "*Radiative decay engineering: the role of*" J. Phys.D.: Appl. Phys. 36 R240 (2003)

photonic mode density in biotechnology

[60] V.A. Shubin, W.Kim, V.P. Safonov, A.K. Sarychev, R.L. Armstrong, V.M. Shalaev, *"Surface-plasmon-enhanced radiation effects in confined photonic systems"* J. Lightwave Tech. 17, 2183 (1999)

[61] P. Anger, P. Bharadwaj, L. Novotny, *"Enhancement and quenching of single-molecule fluorescence"* Phys.Rev.Lett. 96, 113002 (2006)

[62] L.V. Alekseyev, E.E. Narimanov, *Radiative Decay Engineering in Metamaterials*, in *Tutorials in Metamaterials* eds. M. Noginov and V. Podolskiy, CRC press (NY, 2011)

[63] L.V. Alekseyev, E.E. Narimanov, T. Tumkur, H. Li, Y. Barnakov, M. A. Noginov, *Uniaxial epsilon-near-zero metamaterial for angular filtering and polarization control* Appl.Phys.Lett, 97, 131107 (2010)